Computer Methods in Applied Mechanics and Engineering 433 (2025) 117500

Contents lists available at ScienceDirect

Comput. Methods Appl. Mech. Engrg.

journal homepage: www.elsevier.com/locate/cma

Direct serendipity finite elements on cuboidal hexahedra

Todd Arbogast [a,b,*], Chuning Wang [a]

[a] Department of Mathematics, C1200, University of Texas at Austin, Austin, TX 78712, USA
[b] Oden Institute for Computational Engineering and Sciences, C0200, University of Texas at Austin, Austin, TX 78712, USA

ARTICLE INFO

MSC:
65N30
65N12
65N15
65D05

Keywords:
Hexahedral mesh
Serendipity finite elements
Direct finite elements
Conforming finite elements
Optimal approximation
Convergence

ABSTRACT

We construct direct serendipity finite elements on general cuboidal hexahedra, which are H^1-conforming and optimally approximate to any order. The new finite elements are *direct* in that the shape functions are directly defined on the physical element. Moreover, they are *serendipity* by possessing a minimal number of degrees of freedom satisfying the conformity requirement. Their shape function spaces consist of polynomials plus (generally nonpolynomial) supplemental functions, where the polynomials are included for the approximation property and supplements are added to achieve H^1-conformity. The finite elements are fully constructive. The shape function spaces of higher order $r \geq 3$ are developed first, and then the lower order spaces are constructed as subspaces of the third order space. Under a shape regularity assumption, and a mild restriction on the choice of supplemental functions, we develop the convergence properties of the new direct serendipity finite elements. Numerical results with different choices of supplements are compared on two mesh sequences, one regularly distorted and the other one randomly distorted. They all possess a convergence rate that aligns with the theory, while a slight difference lies in their performance.

1. Introduction

The seminal book of Wachspress in 1975 [1] has focused interest in defining H^1-conforming finite elements on polytopal elements, in particular, on polygons and polyhedra. Polytopal meshes have been used in many areas of application with the advantage of its flexibility. For just two examples, in applications to topology optimization [2,3] and fracture propagation [4,5], randomly generated polytopal elements were seen to reduce the bias that is associated to standard meshes.

There are many approaches for numerically solving partial differential equations on polyhedral meshes. Of course, the nonconforming discontinuous Galerkin (DG) methods can be posed on polyhedral meshes [6,7], and this is also the case for the related weak Galerkin methods [8]. An interesting approach to construct finite elements on polytopes is introduced in [9–11] by considering broken ultraweak variational formulations and applying the discontinuous Petrov–Galerkin (DPG) methodology [12]. The discretization applies classical broken test and trial spaces; however, it uses more than the minimal number of degrees of freedom (DoFs) required for H^1-conformity (see Section 3 below). Although the framework is not H^1-conforming for a general polyhedral element, a conforming approximation is provided of any optimal order of accuracy r as long as the elements have triangular or quadrilateral faces.

The mimetic methods, a type of finite volume method, have been defined on polyhedra in [13]. They mimic the properties of the differential operators such as the discrete divergence theorem. However, they represent the solution only at DoFs (i.e., they do not provide a basis for interpolation). The virtual element methods [14] seem to have grown out of the mimetic methods. They do

* Corresponding author.
E-mail addresses: arbogast@oden.utexas.edu (T. Arbogast), wan01937@umn.edu (C. Wang).

https://doi.org/10.1016/j.cma.2024.117500
Received 1 July 2024; Received in revised form 26 August 2024; Accepted 19 October 2024
Available online 30 October 2024

not provide a basis for interpolation but possess a virtual (i.e., not computable) and conforming underlying finite element basis. However, they usually require the addition of a problem dependent stabilization term in the equations to control the unknown virtual components of the solution.

One may desire a conforming approximation with an explicit finite element basis in many instances. The latter is particularly helpful when dealing with nonlinear partial differential equations and coupled systems of equations. They are more fundamental for application since they provide a general framework for interpolation and approximation of functions, independent of how they are used. For example, they could be applied to data interpolation and visualization. However, there are currently not many good H^1-conforming polyhedral finite elements.

Serendipity finite elements defined on cubes by Arnold and Awanou [15], denoted as $S_r(\hat{E})$, $r \geq 1$, are well known to be H^1-conforming and approximate to order $r+1$ with a minimal number of DoFs. However, they lose optimal order accuracy when mapped to a cuboidal hexahedron, which is defined as a three dimensional non-degenerate hexahedron with flat faces that can be obtained by a trilinear map from a reference cube. Tensor product spaces on a cube, on the other hand, maintain optimal approximation properties while mapped to a cuboidal hexahedron. However, they suffer from using an excessive number of DoFs.

In this work, we construct direct serendipity finite elements on a cuboidal hexahedron E, which are of the form

$$\mathcal{DS}_r(E) = \mathbb{P}_r(E) \oplus \mathbb{S}_r^{DS}(E), \quad r \geq 1, \tag{1}$$

where $\mathbb{P}_r(E)$ is the space of polynomials on E up to degree r, and $\mathbb{S}_r^{DS}(E)$ consists of supplemental functions. These supplemental functions cannot in general be polynomials. We give several ways to define them, and one choice results in the supplements being piecewise polynomial on a submesh of the element. The construction is based on the previous work of the authors on developing direct serendipity finite elements for two dimensional convex polygons [16,17]. The complicated geometry of a three dimensional hexahedron makes the construction more subtle and intricate. We develop the approximation properties of the new finite elements, and evaluate their performance through numerical tests. Our work may also provide a methodology for future development of conforming finite elements on more general polyhedra, and possibly $H(\mathrm{curl})$-conforming finite elements on cuboidal hexahedra in the de Rham sequence [18].

One interesting use of our new direct serendipity finite elements is in application to enriched Galerkin (EG) methods [19,20], in which continuous finite elements are enriched with piecewise discontinuous constants to maintain local mass conservation. They have fewer degrees of freedom than DG methods, so they are easier to solve [20]. Implementation using direct serendipity spaces can make the method even more efficient [21].

The rest of the paper is organized as follows. We introduce some notation and preliminaries in Section 2. We count the minimum number of degrees of freedom needed for H^1-conformity in Section 3. The actual construction proceeds by constructing the finite element, independently of conformity considerations, in Sections 4–5. To illustrate the key idea, we first construct the direct serendipity space for $r = 3$ in Section 4. We extend the construction to general higher order $r \geq 3$ cases in Section 5. The lower order $r = 1, 2$ direct serendipity elements are then constructed in Section 6 as subsets of the $r = 3$ case. Section 7 is included to describe how to construct certain special functions needed in Sections 4–5. Returning to the question of conformity, some additional restrictions are introduced in Section 8 to make the finite elements H^1-conforming on the entire domain. We prove the approximation properties in Section 9 and discuss the numerical results in Section 10. Finally, in Section 11 we summarize our results and propose some suggestions for future work.

2. Notation and preliminaries

Let $\mathbb{P}_r(\omega)$ denote the space of polynomials of degree up to r on $\omega \subset \mathbb{R}^d$, where $d = 0$ (a point), 1, 2, or 3. Recall that

$$\dim \mathbb{P}_r(\mathbb{R}^d) = \binom{r+d}{d} = \frac{(r+d)!}{r!\,d!}. \tag{2}$$

Let $\tilde{\mathbb{P}}_r(\omega)$ denote the space of homogeneous polynomials of degree r on ω. Then

$$\dim \tilde{\mathbb{P}}_r(\mathbb{R}^d) = \binom{r+d-1}{d-1} = \frac{(r+d-1)!}{r!\,(d-1)!}, \quad d \geq 1. \tag{3}$$

Let the element $E \subset \mathbb{R}^3$ be a closed, nondegenerate, convex cuboidal hexahedron (i.e., a quadrilaterally-faced hexahedron), with 6 faces, 12 edges, and 8 vertices. The hexahedron E is nondegenerate in that it does not degenerate to any polyhedron with fewer faces, edges, or vertices, neither to a polygon, line segment, nor a point. We choose to identify the faces of E based on the mapping from a reference element $\hat{E}$ as depicted in Fig. 1. Note that this is only for the convenience of indexing.

Let the faces of E be denoted as f_n, $n = \pm1, \pm2, \pm3$. Let the reference element $\hat{E}$ be $[-1, 1]^3$, with faces denoted as $\hat{f}_n$, $n = \pm1, \pm2, \pm3$. Define the trilinear and bijective map $\mathbf{F}_E : \hat{E} \to E$ that maps the faces of $\hat{E}$ to those of E, such that

$$\begin{aligned}
&\hat{f}_{-1} = \hat{E} \cap \{\hat{x} = -1\} \xrightarrow{\mathbf{F}_E} f_{-1}, \quad \hat{f}_1 = \hat{E} \cap \{\hat{x} = 1\} \xrightarrow{\mathbf{F}_E} f_1,\\
&\hat{f}_{-2} = \hat{E} \cap \{\hat{y} = -1\} \xrightarrow{\mathbf{F}_E} f_{-2}, \quad \hat{f}_2 = \hat{E} \cap \{\hat{y} = 1\} \xrightarrow{\mathbf{F}_E} f_2,\\
&\hat{f}_{-3} = \hat{E} \cap \{\hat{z} = -1\} \xrightarrow{\mathbf{F}_E} f_{-3}, \quad \hat{f}_3 = \hat{E} \cap \{\hat{z} = 1\} \xrightarrow{\mathbf{F}_E} f_3.
\end{aligned} \tag{4}$$

For $i = \pm1$, $j = \pm2$, and $k = \pm3$, denote the edges of E as

$$e_{j,k} = f_j \cap f_k, \quad e_{i,k} = f_i \cap f_k, \quad e_{i,j} = f_i \cap f_j, \tag{5}$$

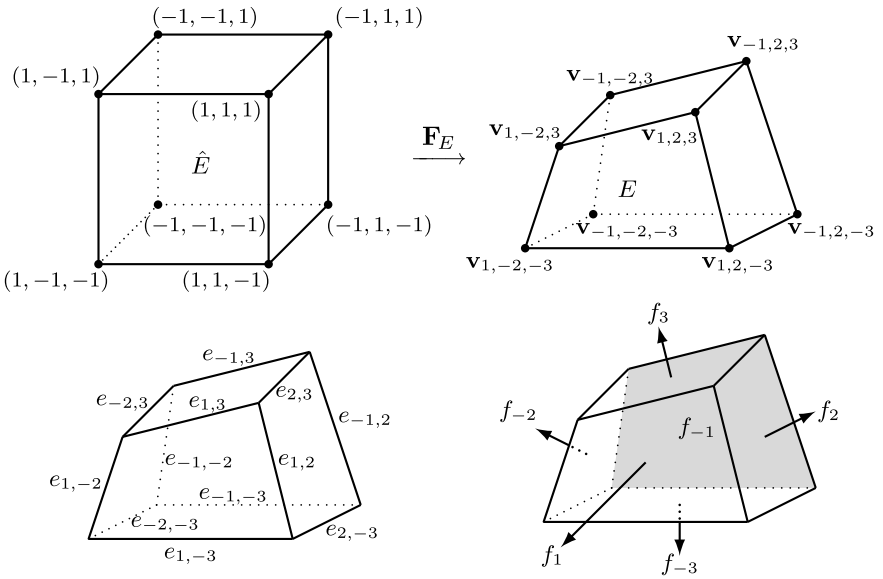

Fig. 1. A reference element $\hat{E} = [-1, 1]^3$ and a cuboidal hexahedron E, with faces $\hat{f}_i$ and f_i, as well as vertices $(-1, -1, -1)$ and $\mathbf{v}_{-1,-2,-3}$, etc., respectively. The notation of each vertex, edge, and face of E is shown correspondingly in the top right picture, the bottom left picture, and the bottom right picture.

and the vertices as $\mathbf{v}_{i,j,k} = f_i \cap f_j \cap f_k$, as shown in Fig. 1. Also let ν_n denote the unit outer normal to face f_n for $n = \pm 1, \pm 2, \pm 3$.

Denote F_E^0 as the pullback map induced from $\mathbf{F}_E^{-1}$. To be more precise, F_E^0 takes a function $\hat{\phi}$ defined on $\hat{E}$ to a function ϕ defined on E by the rule

$$\phi(\mathbf{x}) = F_E^0(\hat{\phi})(\mathbf{x}) = \hat{\phi}(\hat{\mathbf{x}}), \tag{6}$$

where $\mathbf{x} = \mathbf{F}_E(\hat{\mathbf{x}})$. We require special functions R_x, R_y, and R_z satisfying

$$R_x = \begin{cases} -1, & \text{on } f_{-1}, \\ 1, & \text{on } f_1, \end{cases} \quad R_y = \begin{cases} -1, & \text{on } f_{-2}, \\ 1, & \text{on } f_2, \end{cases} \quad R_z = \begin{cases} -1, & \text{on } f_{-3}, \\ 1, & \text{on } f_3. \end{cases} \tag{7}$$

Such functions exist, however, they cannot be polynomials, unless opposite faces are parallel. For instance, these functions could be defined as pullback maps

$$R_x(\mathbf{x}) = \hat{x}, \quad R_y(\mathbf{x}) = \hat{y}, \quad R_z(\mathbf{x}) = \hat{z}, \quad \text{where } \hat{\mathbf{x}} = \mathbf{F}_E^{-1}(\mathbf{x}) = (\hat{x}, \hat{y}, \hat{z}). \tag{8}$$

Alternative constructions will be given later in Section 7.

Define linear functions λ_x, λ_y, and λ_z such that the zero plane $\mathcal{P}_x$ of λ_x intersects the four edges $e_{\pm 2,\pm 3}$, and that of λ_y, denoted as $\mathcal{P}_y$, intersects $e_{\pm 1,\pm 3}$. Similarly, the zero plane of λ_z, denoted as $\mathcal{P}_z$, intersects $e_{\pm 1,\pm 2}$. Notice that for some special geometry, such a definition has a possibility of forming linearly dependent λ_x, λ_y, and λ_z. Taking the cube as an example, note that $\mathbf{v}_{-1,-2,-3}$, $\mathbf{v}_{1,-2,-3}$, $\mathbf{v}_{1,2,3}$, and $\mathbf{v}_{-1,2,3}$ form a plane, and this plane could be taken both as $\mathcal{P}_y$ and $\mathcal{P}_z$. Therefore, we also ask $\mathcal{P}_x$, $\mathcal{P}_y$, and $\mathcal{P}_z$ not to coincide. These linear functions form bases for spaces of polynomials.

Lemma 2.1. *Let the polynomial degree be $r \geq 0$.*

1. *For $i = \pm 1$, $j = \pm 2$, and $k = \pm 3$, $\{\lambda_x^s|_{e_{j,k}},\ s = 0, 1, \dots, r\}$, $\{\lambda_y^s|_{e_{i,k}},\ s = 0, 1, \dots, r\}$, and $\{\lambda_z^s|_{e_{i,j}},\ s = 0, 1, \dots, r\}$ form bases for $\mathbb{P}_r(e_{j,k})$, $\mathbb{P}_r(e_{i,k})$, and $\mathbb{P}_r(e_{i,j})$, respectively.*
2. *For $i = \pm 1$, $j = \pm 2$, and $k = \pm 3$, $\{\lambda_y^{s_1}\lambda_z^{s_2}|_{f_i}, 0 \leq s_1 + s_2 \leq r\}$, $\{\lambda_x^{s_1}\lambda_z^{s_2}|_{f_j}, 0 \leq s_1 + s_2 \leq r\}$, and $\{\lambda_x^{s_1}\lambda_y^{s_2}|_{f_k}, 0 \leq s_1 + s_2 \leq r\}$ form bases for $\mathbb{P}_r(f_i)$, $\mathbb{P}_r(f_j)$, and $\mathbb{P}_r(f_k)$, respectively.*
3. *The polynomials $\lambda_x^{s_1}\lambda_y^{s_2}\lambda_z^{s_3}$ with $0 \leq s_1 + s_2 + s_3 \leq r$ form a basis for $\mathbb{P}_r(E)$.*

Proof. *Part 1.* By construction, $e_{j,k} \nparallel \mathcal{P}_x$ for $j = \pm 2$ and $k = \pm 3$, so $\lambda_x|_{e_{j,k}}$ is linear with nonzero slope. Therefore, its powers λ_x^s with $s = 0, 1, \dots, r$ form a basis for $\mathbb{P}_r(e_{j,k})$. The proof for the other edges follows by symmetry.

Part 2. We need to show that if $p = \sum_{s_2=0}^{r} \sum_{s_1=0}^{r-s_2} c_{s_1,s_2} \lambda_y^{s_1} \lambda_z^{s_2} = 0$ on f_i for $i = -1$ or 1, then $c_{s_1,s_2} = 0$, $\forall 0 \leq s_1 + s_2 \leq r$. Recall that $\lambda_y|_{\mathcal{P}_y} = \lambda_z|_{\mathcal{P}_z} = 0$, and both $\mathcal{P}_y$ and $\mathcal{P}_z$ intersects f_i along some line. Therefore,

$$p|_{f_i \cap \mathcal{P}_y} = \sum_{s_2=0}^{r} c_{0,s_2} \lambda_z^{s_2} = 0, \tag{9}$$

$$p|_{f_i\cap\mathcal{P}_z} = \sum_{s_1=0}^{r} c_{s_1,0}\lambda_y^{s_1} = 0. \tag{10}$$

We conclude $c_{0,s_2} = c_{s_1,0} = 0$, $\forall s_1, s_2 = 0, 1, \dots, r$ using part 1 of the lemma. Now we have

$$p = \sum_{s_2=1}^{r-1}\sum_{s_1=1}^{r-s_2} c_{s_1,s_2}\lambda_y^{s_1}\lambda_z^{s_2} = \lambda_y\lambda_z\, p_1, \quad p_1 = \sum_{s_2=1}^{r-1}\sum_{s_1=1}^{r-s_2} c_{s_1,s_2}\lambda_y^{s_1-1}\lambda_z^{s_2-1}. \tag{11}$$

By $\lambda_y\lambda_z \neq 0$ in the interior of f_i, $p|_{f_i} = 0$ is equivalent to $p_1|_{f_i} = 0$. Therefore,

$$p_1|_{f_i\cap\mathcal{P}_y} = \sum_{s_2=1}^{r-1} c_{1,s_2}\lambda_z^{s_2-1} = 0, \tag{12}$$

$$p_1|_{f_i\cap\mathcal{P}_z} = \sum_{s_1=1}^{r-1} c_{s_1,1}\lambda_y^{s_1-1} = 0, \tag{13}$$

and again in analogy to part 1 of the lemma (for $r-2$) shows $c_{1,s_2} = c_{s_1,1} = 0$, $\forall s_1, s_2 = 1, 2, \dots, r-1$. We can continue the argument and finally obtain $c_{s_1,s_2} = 0$ for all $0 \le s_1 + s_2 \le r$. The proof for the bases on the other faces follows by symmetry.

Part 3. The idea of proof for part 3 is the same as in part 2, where we restrict the polynomial to a lower dimensional object. If on E we have

$$\sum_{0\le s_1+s_2+s_3\le r} c_{s_1,s_2,s_3}\lambda_x^{s_1}\lambda_y^{s_2}\lambda_z^{s_3} = 0, \tag{14}$$

then we must have on $\mathcal{P}_x$, where $\lambda_x = 0$, only terms with $s_1 = 0$, i.e.,

$$\sum_{0\le s_2+s_3\le r} c_{0,s_2,s_3}\lambda_y^{s_2}\lambda_z^{s_3} = 0. \tag{15}$$

By a similar proof as in part 2 for faces, we can also show that $\{\lambda_y^{s_2}\lambda_z^{s_3}|_{\mathcal{P}_x}, 0 \le s_2 + s_3 \le r\}$ forms a basis for $\mathbb{P}_r(\mathcal{P}_x)$. Therefore, in (14), $c_{0,s_2,s_3} = 0$, and similarly, $c_{s_1,0,s_3} = c_{s_1,s_2,0} = 0$. Then

$$p = \sum_{s_3=1}^{r-2}\sum_{s_2=1}^{r-1-s_3}\sum_{s_1=1}^{r-s_2-s_3} c_{s_1,s_2,s_3}\lambda_x^{s_1}\lambda_y^{s_2}\lambda_z^{s_3} = \lambda_x\lambda_y\lambda_z\, p_1, \tag{16}$$

$$p_1 = \sum_{s_3=1}^{r-2}\sum_{s_2=1}^{r-1-s_3}\sum_{s_1=1}^{r-s_2-s_3} c_{s_1,s_2,s_3}\lambda_x^{s_1-1}\lambda_y^{s_2-1}\lambda_z^{s_3-1}.$$

We repeat the previous step of restricting the function to $\mathcal{P}_x$, $\mathcal{P}_y$, and $\mathcal{P}_z$, obtaining that $c_{1,s_2,s_3} = c_{s_1,1,s_3} = c_{s_1,s_2,1} = 0$. Continuing this procedure, we finally conclude that all the coefficients are zero. □

Finally, define λ_n as the distance of a point to the face f_n,

$$\lambda_n(\mathbf{x}) = -(\mathbf{x} - \mathbf{x}_{f_n})\cdot \nu_n, \quad n = \pm1, \pm2, \pm3, \tag{17}$$

where $\mathbf{x}_{f_n}$ is any point on the face f_n. Note that λ_n does not depend on the choice of $\mathbf{x}_{f_n}$. Later, in Section 4 we will need to understand the restriction of λ_n for $n \in \{\pm1, \pm2, \pm3\}$ to the edges.

Lemma 2.2. *For $i = \pm1$, $j = \pm2$, $k = \pm3$ and $n \in \{\pm1, \pm2, \pm3\}$, let $A_{n,x}^{j,k}$, $A_{n,y}^{i,k}$, and $A_{n,z}^{i,j}$ satisfy*

$$\lambda_n|_{e_{j,k}} = A_{n,x}^{j,k} + B_{n,x}^{j,k}\lambda_x|_{e_{j,k}}, \tag{18}$$

$$\lambda_n|_{e_{i,k}} = A_{n,y}^{i,k} + B_{n,y}^{i,k}\lambda_y|_{e_{i,k}}, \tag{19}$$

$$\lambda_n|_{e_{i,j}} = A_{n,z}^{i,j} + B_{n,z}^{i,j}\lambda_z|_{e_{i,j}}. \tag{20}$$

Then $A_{-j,x}^{j,k}$, $A_{-k,x}^{j,k}$, $A_{-i,y}^{i,k}$, $A_{-k,y}^{i,k}$, $A_{-i,z}^{i,j}$, and $A_{-j,z}^{i,j}$ are strictly positive.

Proof. By Lemma 2.1, it is possible to define the restriction of λ_n on each edge in the form (18)–(20). The strict positivity of $A_{-j,x}^{j,k}$, $A_{-k,x}^{j,k}$, $A_{-i,y}^{i,k}$, $A_{-k,y}^{i,k}$, $A_{-i,z}^{i,j}$, and $A_{-j,z}^{i,j}$ is due to the geometry of a convex hexahedron. □

In Section 5, we will also need to understand the restriction of λ_n to the faces.

Lemma 2.3. *For $n \in \{\pm1, \pm2, \pm3\}$, the following expressions hold for appropriate coefficients:*

$$\lambda_n|_{f_{\pm1}} = A_{n,yz}^{\pm1} + B_{n,yz}^{\pm1}\lambda_y|_{f_{\pm1}} + C_{n,yz}^{\pm1}\lambda_z|_{f_{\pm1}}; \tag{21}$$

$$\lambda_n|_{f_{\pm2}} = A_{n,xz}^{\pm2} + B_{n,xz}^{\pm2}\lambda_x|_{f_{\pm2}} + C_{n,xz}^{\pm2}\lambda_z|_{f_{\pm2}}; \tag{22}$$

$$\lambda_n|_{f_{\pm3}} = A_{n,xy}^{\pm3} + B_{n,xy}^{\pm3}\lambda_x|_{f_{\pm3}} + C_{n,xy}^{\pm3}\lambda_y|_{f_{\pm3}}. \tag{23}$$

Moreover, $A_{-1,yz}^{1}$, $A_{1,yz}^{-1}$, $A_{-2,xz}^{2}$, $A_{2,xz}^{-2}$, $A_{-3,xy}^{3}$, and $A_{3,xy}^{-3}$ are strictly positive.

Table 1
Geometric decomposition and number of degrees of freedom (DoFs) associated to each geometric object of a cuboidal hexahedron E for a serendipity element of index $r \geq 1$.

Dim.	Object name	Object count	DoFs per object	Total DoFs
0	Vertex	8	1	8
1	Edge	12	$\dim \mathbb{P}_{r-2}(\mathbb{R})$	$12(r-1)$
2	Face	6	$\dim \mathbb{P}_{r-4}(\mathbb{R}^2)$	$3(r-2)(r-3)$, if $r \geq 2$
3	Interior	1	$\dim \mathbb{P}_{r-6}(\mathbb{R}^3)$	$\frac{1}{6}(r-3)(r-4)(r-5)$, if $r \geq 3$

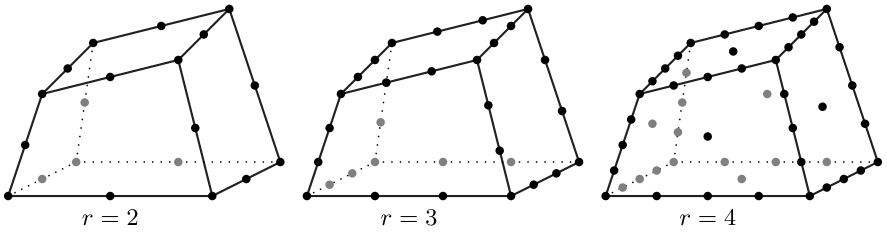

Fig. 2. Degrees of freedom (DoFs) for a serendipity element of index $r = 2$, 3, and 4. The DoFs are expressed as dots, as if they were nodal DoFs. They appear at the vertices, in the interior of the edges, and in the interior of the faces (DoFs in the element interior do not appear until $r = 6$).

The proof is similar to that for the previous lemma.

To conclude this section, we recall from Ciarlet's definition [22] of a finite element $(E, \mathcal{P}, \mathcal{N})$ that we need $\mathcal{P}$, a finite-dimensional space of functions on E, and $\mathcal{N} = \{N_1, N_2, \dots, N_{\dim \mathcal{P}}\}$, a basis for $\mathcal{P}'$, for which the members are referred to as degrees of freedom (DoFs). That $\mathcal{N}$ is a basis for $\mathcal{P}'$ is equivalent to saying that the DoFs are unisolvent, i.e., if $\psi \in \mathcal{P}$ satisfies $N_j(\psi) = 0$, $\forall j = 1, 2, \dots, \dim \mathcal{P}$, then $\psi = 0$. According to Ciarlet, the issue of global conformity over the domain should be addressed after the finite elements are defined, which we do in Section 8.

3. Geometric decomposition and degrees of freedom

For approximation purposes, we ask that $\mathbb{P}_r(E) \subset \mathcal{DS}_r(E)$. The total number of DoFs required for H^1-conformity can be determined by a geometric decomposition of E as given in Table 1. These required DoFs are illustrated in Fig. 2. The total number of DoFs for $r = 1$ and $r = 2$ is

$$D_r = \begin{cases} 8 = \dim \mathbb{P}_1(E) + 4, & \text{if } r = 1, \\ 20 = \dim \mathbb{P}_2(E) + 10, & \text{if } r = 2, \end{cases} \tag{24}$$

which means we need 4 linearly independent supplements for $\mathcal{DS}_1(E)$ and 10 for $\mathcal{DS}_2(E)$. When $r \geq 3$, the total number of DoFs is

$$\begin{aligned} D_r &= 8 + 12(r-1) + 3(r-2)(r-3) + \frac{1}{6}(r-3)(r-4)(r-5) \\ &= \dim \mathbb{P}_r(E) + 3(r+1). \end{aligned} \tag{25}$$

We view $\mathcal{DS}_1(E)$ and $\mathcal{DS}_2(E)$ as special cases, and start with the construction for $r \geq 3$, where we need to define exactly $3(r+1)$ linearly independent supplemental functions. We have many choices, and each choice give a unique serendipity space. In this paper, we give particular constructions, and show their conformity and unisolvence.

The DoFs for $\phi \in \mathcal{DS}_r(E)$ are given by

$$\phi(\mathbf{v}), \qquad \text{for all the vertices } \mathbf{v}, \tag{26}$$

$$\int_e \phi\, q, \quad \forall q \in \mathbb{P}_{r-2}(e), \qquad \text{for all the edges } e, \tag{27}$$

$$\int_f \phi\, q, \quad \forall q \in \mathbb{P}_{r-4}(f), \qquad \text{for all the faces } f, \tag{28}$$

$$\int_E \phi\, q, \quad \forall q \in \mathbb{P}_{r-6}(E). \tag{29}$$

The unisolvence of the DoFs will be clear after we construct the basis functions. Note that we can also take DoFs to be nodal evaluation, and construct the corresponding nodal basis functions. These will assist the development of the approximation theory later in Section 9.

4. Finite element space and basis functions for $r = 3$

We illustrate our finite elements with an explicit construction for the simplest case $r = 3$, which has 32 DoFs, including 8 vertex DoFs and 24 edge DoFs. For vertex DoFs, the corresponding basis functions $\phi^{\mathbf{v}}_{i,j,k}$, where $i = \pm1$, $j = \pm2$, and $k = \pm3$, will be defined later such that

$$\phi^{\mathbf{v}}_{i,j,k}(\mathbf{x}) = \begin{cases} 1 & \text{at } \mathbf{v}_{i,j,k}, \\ 0 & \text{at all the other vertices.} \end{cases} \tag{30}$$

Edges and their DoFs are divided into three sets of 4 edges between opposite faces. For $i = \pm1, j = \pm2, k = \pm3$, and $s = 0, 1$, denote the corresponding basis functions for each set of DoFs as $\phi^e_{i,j;s}$, $\phi^e_{j,k;s}$, and $\phi^e_{i,k;s}$ respectively. These will be defined later so that

$$\phi^e_{j,k;s}(\mathbf{x}) = \begin{cases} \lambda_{-1}\lambda_1\lambda_x^s, & \forall \mathbf{x} \in e_{j,k}, \\ 0, & \forall \mathbf{x} \in f_n, \quad n \neq j, k. \end{cases} \tag{31}$$

$$\phi^e_{i,k;s}(\mathbf{x}) = \begin{cases} \lambda_{-2}\lambda_2\lambda_y^s, & \forall \mathbf{x} \in e_{i,k}, \\ 0, & \forall \mathbf{x} \in f_n, \quad n \neq i, k. \end{cases} \tag{32}$$

$$\phi^e_{i,j;s}(\mathbf{x}) = \begin{cases} \lambda_{-3}\lambda_3\lambda_z^s, & \forall \mathbf{x} \in e_{i,j}, \\ 0, & \forall \mathbf{x} \in f_n, \quad n \neq i, j. \end{cases} \tag{33}$$

The set of these functions are linearly independent according to Lemma 2.1.

The finite element requires a supplemental function space $\mathbb{S}_3^{DS}(E)$ such that

$$\begin{aligned} DS_3(E) &= \mathbb{P}_3(E) \oplus \mathbb{S}_3^{DS}(E) \\ &= \operatorname{span}\{\phi^{\mathbf{v}}_{i,j,k},\ \phi^e_{j,k;s},\ \phi^e_{i,k;s},\ \phi^e_{i,j;s} \mid i = \pm1,\ j = \pm2,\ k = \pm3,\ s = 0, 1\}. \end{aligned} \tag{34}$$

4.1. The serendipity space on a cube

We first review the construction of $DS_3(\hat{E})$ for $\hat{E} = [-1, 1]^3$ a cube [15]. The vertex basis function $\phi^{\mathbf{v}}_{i,j,k}$ with the property (30) is

$$\phi^{\mathbf{v}}_{i,j,k}(\hat{x}, \hat{y}, \hat{z}) = \frac{1}{8}(1 + \operatorname{sign}(i)\hat{x})(1 + \operatorname{sign}(j)\hat{y})(1 + \operatorname{sign}(k)\hat{z}) \in \mathbb{P}_3, \tag{35}$$

with the sign function defined as $\operatorname{sign}(i) = i/|i|$. For edge basis functions, we present those for the DoFs on $\hat{e}_{\pm1,\pm2}$ as an example. If $i = \pm1$ and $j = \pm2$, the two edge basis functions $\phi^e_{i,j;s}$ for $s = 0, 1$ are defined as

$$\phi^e_{i,j;s}(\hat{x}, \hat{y}, \hat{z}) = \frac{1}{4}\hat{z}^s(1 - \hat{z}^2)(1 + \operatorname{sign}(i)\hat{x})(1 + \operatorname{sign}(j)\hat{y}) \in \mathbb{P}_5. \tag{36}$$

All the vertex basis functions are in $\mathbb{P}_3(\hat{E})$ and require no supplemental functions. However, in the construction of $\phi^e_{\pm1,\pm2;1}$, there are 3 supplemental functions which are linearly independent polynomials with degree greater than $r = 3$, namely

$$\hat{z}(1 - \hat{z}^2)\{\hat{x},\ \hat{y},\ \hat{x}\hat{y}\}. \tag{37}$$

The construction of $\phi^e_{\pm1,\pm2;0}$, has one polynomial with the highest degree greater than $r = 3$, which is

$$(1 - \hat{z}^2)\hat{x}\hat{y}. \tag{38}$$

Similarly, there are 4 different supplemental functions needed for constructing $\phi^e_{\pm1,\pm3;s}$, $s = 0, 1$, and also 4 more for $\phi^e_{\pm2,\pm3;s}$, $s = 0, 1$. All of these 32 basis functions belong to the space $\mathbb{P}_3(\hat{E}) \oplus \mathbb{S}_3^{DS}(\hat{E})$, and they form a linearly independent set, since each corresponds to a different degree of freedom.

4.2. Vertex basis functions

The next step is to generalize the construction to a cuboidal hexahedron E. It is straightforward to generalize the eight vertex basis functions as

$$\phi^{\mathbf{v}}_{i,j,k}(\mathbf{x}) = \frac{\lambda_{-i}(\mathbf{x})\lambda_{-j}(\mathbf{x})\lambda_{-k}(\mathbf{x})}{\lambda_{-i}(\mathbf{v}_{i,j,k})\lambda_{-j}(\mathbf{v}_{i,j,k})\lambda_{-k}(\mathbf{v}_{i,j,k})} \in \mathbb{P}_3, \tag{39}$$

for $i = \pm1$, $j = \pm2$, and $k = \pm3$.

4.3. Supplemental functions

In accordance with the serendipity element for a reference cube, the 24 edge basis functions are divided into 3 groups $\phi^e_{\pm1,\pm2;s}$, $\phi^e_{\pm1,\pm3;s}$, and $\phi^e_{\pm2,\pm3;s}$. The construction of each group will involve four supplements, of which three functions are for $s = 1$, and one function is for $s = 0$.

On a cube, the serendipity element restricted to any lower-dimensional geometry object coincides with a serendipity element defined directly on that object [15]. We aim to construct $\phi^e_{j,k;s}$, $\phi^e_{i,k;s}$, and $\phi^e_{i,j;s}$ on a cuboidal hexahedron in such a way that they restrict to a 2D direct serendipity space on each face. The 2D direct serendipity spaces are defined in [16], and these are, for any $r \geq 2$,

$$\mathcal{DS}^{(2)}_r(f_i) = \mathbb{P}_r(f_i) \oplus \operatorname{span}\{\lambda_{-2}\lambda_2\lambda_y^{r-2}R_z,\ \lambda_{-3}\lambda_3\lambda_z^{r-2}R_y\}|_{f_i},\ \ i = \pm1, \tag{40}$$

$$\mathcal{DS}^{(2)}_r(f_j) = \mathbb{P}_r(f_j) \oplus \operatorname{span}\{\lambda_{-1}\lambda_1\lambda_x^{r-2}R_z,\ \lambda_{-3}\lambda_3\lambda_z^{r-2}R_x\}|_{f_j},\ \ j = \pm2, \tag{41}$$

$$\mathcal{DS}^{(2)}_r(f_k) = \mathbb{P}_r(f_k) \oplus \operatorname{span}\{\lambda_{-1}\lambda_1\lambda_x^{r-2}R_y,\ \lambda_{-2}\lambda_2\lambda_y^{r-2}R_x\}|_{f_k},\ k = \pm3. \tag{42}$$

From the cube, we extend the construction naturally in (36) for $s = 1$ to

$$\phi^e_{j,k;1} = \frac{1}{4}\lambda_x\lambda_{-1}\lambda_1(1 + \operatorname{sign}(j)R_y)(1 + \operatorname{sign}(k)R_z), \tag{43}$$

$$\phi^e_{i,k;1} = \frac{1}{4}\lambda_y\lambda_{-2}\lambda_2(1 + \operatorname{sign}(i)R_x)(1 + \operatorname{sign}(k)R_z), \tag{44}$$

$$\phi^e_{i,j;1} = \frac{1}{4}\lambda_z\lambda_{-3}\lambda_3(1 + \operatorname{sign}(i)R_x)(1 + \operatorname{sign}(j)R_y), \tag{45}$$

which are zero on all the faces except for $f_j \cup f_k$, $f_i \cup f_k$, and $f_i \cup f_j$, respectively, and have the required property that their restrictions on each face f_n lie in $\mathcal{DS}^{(2)}_3(f_n)$ for all $n \in \{\pm1, \pm2, \pm3\}$. We have used three supplements for each group in the construction of (43)–(45), which are identified as

$$\lambda_x\lambda_{-1}\lambda_1\{R_y,\ R_z,\ R_yR_z\}, \tag{46}$$

$$\lambda_y\lambda_{-2}\lambda_2\{R_x,\ R_z,\ R_xR_z\}, \tag{47}$$

$$\lambda_z\lambda_{-3}\lambda_3\{R_x,\ R_y,\ R_xR_y\}. \tag{48}$$

Unfortunately, (38) does not naturally generalize so that the restrictions $\phi^e_{j,k;0}|_{f_n}$, $\phi^e_{i,k;0}|_{f_n}$, and $\phi^e_{i,j;0}|_{f_n}$ belong to $\mathcal{DS}^{(2)}_3(f_n)$ for all $n \in \{\pm1, \pm2, \pm3\}$. We require functions ψ_x, ψ_y, and ψ_z with special properties. For ψ_x we require that

$$\psi_x|_{f_{-2}\cup f_{-3}} = 0, \quad \lambda_{-1}\lambda_1\psi_x|_{f_2} \in \mathcal{DS}^{(2)}(f_2),$$
$$\lambda_{-1}\lambda_1\psi_x|_{f_3} \in \mathcal{DS}^{(2)}(f_3), \quad \psi_x|_{e_{2,3}} = 1.$$

Because the face direct serendipity spaces are well defined, knowing ψ_x on the edges determines it on the faces $f_{\pm2}$ and $f_{\pm3}$ of the element. Similar properties need to hold for ψ_y and ψ_z, especially that $\psi_y|_{e_{1,3}} = \psi_z|_{e_{1,2}} = 1$. To be precise, in terms of the coefficients introduced in Lemma 2.2, these functions satisfy on the faces

$$\psi_x = \begin{cases} \psi_{x,2} = \dfrac{1}{A^{2,3}_{-3,x}}\left(\lambda_{-3} - \frac{1}{2}B^{2,3}_{-3,x}\,\lambda_x(1 + R_z)\right), & \text{on } f_2, \\ \psi_{x,3} = \dfrac{1}{A^{2,3}_{-2,x}}\left(\lambda_{-2} - \frac{1}{2}B^{2,3}_{-2,x}\,\lambda_x(1 + R_y)\right), & \text{on } f_3, \\ 0, & \text{on } f_{-2} \cup f_{-3}, \end{cases} \tag{49}$$

$$\psi_y = \begin{cases} \psi_{y,1} = \dfrac{1}{A^{1,3}_{-3,y}}\left(\lambda_{-3} - \frac{1}{2}B^{1,3}_{-3,y}\,\lambda_y(1 + R_z)\right), & \text{on } f_1, \\ \psi_{y,3} = \dfrac{1}{A^{1,3}_{-1,y}}\left(\lambda_{-1} - \frac{1}{2}B^{1,3}_{-1,y}\,\lambda_y(1 + R_x)\right), & \text{on } f_3, \\ 0, & \text{on } f_{-1} \cup f_{-3}, \end{cases} \tag{50}$$

$$\psi_z = \begin{cases} \psi_{z,1} = \dfrac{1}{A^{1,2}_{-2,z}}\left(\lambda_{-2} - \frac{1}{2}B^{1,2}_{-2,z}\,\lambda_z(1 + R_y)\right), & \text{on } f_1, \\ \psi_{z,2} = \dfrac{1}{A^{1,2}_{-1,z}}\left(\lambda_{-1} - \frac{1}{2}B^{1,2}_{-1,z}\,\lambda_z(1 + R_x)\right), & \text{on } f_2, \\ 0, & \text{on } f_{-1} \cup f_{-2}. \end{cases} \tag{51}$$

We have the interior left to be filled in. This will be discussed later in Section 7.

Continuing, we represent $\phi^e_{2,3;0}$, $\phi^e_{1,3;0}$, and $\phi^e_{1,2;0}$ as

$$\phi^e_{2,3;0} = \lambda_{-1}\lambda_1\psi_x, \quad \phi^e_{1,3;0} = \lambda_{-2}\lambda_2\psi_y, \quad \phi^e_{1,2;0} = \lambda_{-3}\lambda_3\psi_z, \tag{52}$$

which equal $\lambda_{-1}\lambda_1$ on $e_{2,3}$, $\lambda_{-2}\lambda_2$ on $e_{1,3}$, and $\lambda_{-3}\lambda_3$ on $e_{1,2}$, respectively. Moreover, their restrictions on faces belong to the corresponding 2D serendipity spaces described in (40)–(42), and they are zero on all the faces other than $f_2 \cup f_3$, $f_1 \cup f_3$, and $f_1 \cup f_2$, respectively. Since only one additional supplemental function for each group is allowed to construct all the $\phi^e_{j,k;0}$, $\phi^e_{i,k;0}$ and $\phi^e_{i,j;0}$, we take (52) as the additional supplements. We get the supplemental space of dimension 12

$$\begin{aligned}\mathbb{S}_3^{DS}(E) = {}& \lambda_{-1}\lambda_1\lambda_x \operatorname{span}\{R_y, R_z, R_yR_z\} \oplus \lambda_{-2}\lambda_2\lambda_y \operatorname{span}\{R_x, R_z, R_xR_z\} \\ & \oplus \lambda_{-3}\lambda_3\lambda_z \operatorname{span}\{R_x, R_y, R_xR_y\} \oplus \operatorname{span}\{\phi^e_{1,2;0}, \phi^e_{1,3;0}, \phi^e_{2,3;0}\}.\end{aligned} \tag{53}$$

4.4. Edge basis functions

We now describe how to construct edge basis functions for $\mathcal{DS}_3(E)$ satisfying (31)–(33). For simplicity, we consider first the group of 8 basis functions $\phi^e_{i,j;s}$ for $i = \pm 1$, $j = \pm 2$, $s = 0, 1$. The four functions $\phi^e_{i,j;1}$ are given in (45). We also have the supplemental function $\phi^e_{1,2;0}$ described in (52). For each group of 4 edges (that lie between a pair of opposite faces), we need 3 more basis functions, which will each be formed as a linear combination of $\phi^e_{1,2;0}$, $\phi^e_{\pm 1,\pm 2;1}$, and some polynomials in $\mathbb{P}_3(E)$.

In fact, we need to take

$$\begin{aligned}\phi^e_{-1,2;0} &= \frac{1}{A^{-1,2}_{-2,z}}\left[\lambda_{-3}\lambda_3\lambda_{-2} - A^{1,2}_{-2,z}\phi^e_{1,2;0} - B^{1,2}_{-2,z}\phi^e_{1,2;1} - B^{-1,2}_{-2,z}\phi^e_{-1,2;1}\right] \\ &= \frac{\lambda_{-3}\lambda_3}{A^{-1,2}_{-2,z}}\Big[\,\lambda_{-2} - A^{1,2}_{-2,z}\psi_z - \tfrac{1}{4}B^{1,2}_{-2,z}\lambda_z(1+R_x)(1+R_y) \\ &\qquad\qquad - \tfrac{1}{4}B^{-1,2}_{-2,z}\lambda_z(1-R_x)(1+R_y)\,\Big],\end{aligned} \tag{54}$$

using (52) and (45). It is not difficult to verify that $\phi^e_{-1,2;0} \in \mathcal{DS}_3(E)$ has the properties required in (33). It clearly vanishes on the faces $f_{\pm 3}$. Using (20), it also vanishes on edges $e_{\pm 1,-2}$ and $e_{1,2}$, and it has the value $\lambda_{-3}\lambda_3$ on edge $e_{-1,2}$. But by construction, $\phi^e_{-1,2;0}$ restricted to a face f_n lies in $\mathcal{DS}^{(2)}_3(f_n)$, which has only edge and vertex DoFs. Thus we conclude that $\phi^e_{-1,2;0}$ vanishes on all the faces not containing edge $e_{-1,2}$, i.e., on all the faces but f_{-1} and f_2.

By a similar procedure, we also get the basis function of order $s = 0$ for $e_{1,-2}$

$$\phi^e_{1,-2;0} = \frac{1}{A^{1,-2}_{-1,z}}(\lambda_{-3}\lambda_3\lambda_{-1} - A^{1,2}_{-1,z}\phi^e_{1,2;0} - B^{1,2}_{-1,z}\phi^e_{1,2;1} - B^{1,-2}_{-1,z}\phi^e_{1,-2;1}). \tag{55}$$

We can obtain $\phi^e_{-1,-2;0}$ using a similar procedure, but it is simpler to realize that

$$\phi^e_{-1,-2;0} = \lambda_{-3}\lambda_3 - \phi^e_{1,2;0} - \phi^e_{-1,2;0} - \phi^e_{1,-2;0}. \tag{56}$$

For the 16 remaining edge basis functions, we have $\phi^e_{j,k;1}$ and $\phi^e_{i,k;1}$ from (43)–(44), as well as $\phi^e_{2,3;0}$ and $\phi^e_{1,3;0}$ from (52), and we can construct

$$\phi^e_{-2,3;0} = \frac{1}{A^{-2,3}_{-3,x}}(\lambda_{-1}\lambda_1\lambda_{-3} - A^{2,3}_{-3,x}\phi^e_{2,3;0} - B^{2,3}_{-3,x}\phi^e_{2,3;1} - B^{-2,3}_{-3,x}\phi^e_{-2,3;1}), \tag{57}$$

$$\phi^e_{2,-3;0} = \frac{1}{A^{2,-3}_{-2,x}}(\lambda_{-1}\lambda_1\lambda_{-2} - A^{2,3}_{-2,x}\phi^e_{2,3;0} - B^{2,3}_{-2,x}\phi^e_{2,3;1} - B^{2,-3}_{-2,x}\phi^e_{2,-3;1}), \tag{58}$$

$$\phi^e_{-1,3;0} = \frac{1}{A^{-1,3}_{-3,y}}(\lambda_{-2}\lambda_2\lambda_{-3} - A^{1,3}_{-3,y}\phi^e_{1,3;0} - B^{1,3}_{-3,y}\phi^e_{1,3;1} - B^{-1,3}_{-3,y}\phi^e_{-1,3;1}), \tag{59}$$

$$\phi^e_{1,-3;0} = \frac{1}{A^{1,-3}_{-1,y}}(\lambda_{-2}\lambda_2\lambda_{-1} - A^{1,3}_{-1,y}\phi^e_{1,3;0} - B^{1,3}_{-1,y}\phi^e_{1,3;1} - B^{1,-3}_{-1,y}\phi^e_{1,-3;1}). \tag{60}$$

Finally, we get $\phi^e_{-2,-3;0}$ and $\phi^e_{-1,-3;0}$ by

$$\phi^e_{-2,-3;0} = \lambda_{-1}\lambda_1 - \phi^e_{2,3;0} - \phi^e_{-2,3;0} - \phi^e_{2,-3;0}, \tag{61}$$

$$\phi^e_{-1,-3;0} = \lambda_{-2}\lambda_2 - \phi^e_{1,3;0} - \phi^e_{-1,3;0} - \phi^e_{1,-3;0}. \tag{62}$$

4.5. Remarks on the construction

The formulation of vertex and edge basis functions naturally gives the unisolvence of the DoFs. Moreover, all the basis functions belong to the space $\mathbb{P}_3(E) \oplus \mathbb{S}_3^{DS}(E)$, and they are linearly independent. We conclude that (34) holds by a dimension counting argument with $\mathbb{S}_3^{DS}(E)$ defined in (53).

Note that our construction starts from asking $\phi^e_{1,2;0}$ to be $\lambda_{-3}\lambda_3$ on $e_{1,2}$, and 0 on f_{-1} and f_{-2}, which loses symmetry. However, there is actually no difference on each face, even if we start the construction from a different edge $e_{i,j}$, $i = \pm 1$, $j = \pm 2$. This is because all the $\phi^e_{i,j;0}$ must satisfy the property that

$$\phi^e_{i,j;0} \begin{cases} \in \lambda_{-3}\lambda_3(\mathbb{P}_1(f_i) \oplus \{\lambda_z R_y\}), & \text{on } f_i, \\ \in \lambda_{-3}\lambda_3(\mathbb{P}_1(f_j) \oplus \{\lambda_z R_x\}), & \text{on } f_j, \\ = 1, & \text{on } f_i \cap f_j = e_{i,j}, \\ = 0, & \text{on } f_n, \quad n \neq i, j. \end{cases} \tag{63}$$

Such a function is uniquely defined up to its values in the interior.

5. Finite element space and basis functions for $r \geq 3$

We can now present the finite element space analogous to (53) when $r \geq 3$. Among all the supplements, $3(r-3)$ of them are zero on all the edges, and we define them as

$$\phi^f_{x,s} = \lambda_{-2}\lambda_2\lambda_{-3}\lambda_3 R_x \lambda_y^s \lambda_z^{r-4-s}, \tag{64}$$

$$\phi^f_{y,s} = \lambda_{-1}\lambda_1\lambda_{-3}\lambda_3 R_y \lambda_x^s \lambda_z^{r-4-s}, \tag{65}$$

$$\phi^f_{z,s} = \lambda_{-1}\lambda_1\lambda_{-2}\lambda_2 R_z \lambda_x^s \lambda_y^{r-4-s}, \tag{66}$$

with $s = 0, 1, \dots, r-4$. The remaining 12 supplements are defined as

$$\phi^e_{x,1} = \lambda_{-1}\lambda_1\lambda_x^{r-2}R_y, \quad \phi^e_{y,1} = \lambda_{-2}\lambda_2\lambda_y^{r-2}R_x, \quad \phi^e_{z,1} = \lambda_{-3}\lambda_3\lambda_z^{r-2}R_x, \tag{67}$$

$$\phi^e_{x,2} = \lambda_{-1}\lambda_1\lambda_x^{r-2}R_z, \quad \phi^e_{y,2} = \lambda_{-2}\lambda_2\lambda_y^{r-2}R_z, \quad \phi^e_{z,2} = \lambda_{-3}\lambda_3\lambda_z^{r-2}R_y, \tag{68}$$

$$\phi^e_{x,3} = \lambda_{-1}\lambda_1\lambda_x^{r-2}R_yR_z, \ \phi^e_{y,3} = \lambda_{-2}\lambda_2\lambda_y^{r-2}R_xR_z, \ \phi^e_{z,3} = \lambda_{-3}\lambda_3\lambda_z^{r-2}R_xR_y, \tag{69}$$

$$\phi^e_{x,4} = \lambda_{-1}\lambda_1\lambda_x^{r-3}\psi_x, \quad \phi^e_{y,4} = \lambda_{-2}\lambda_2\lambda_y^{r-3}\psi_y, \quad \phi^e_{z,4} = \lambda_{-3}\lambda_3\lambda_z^{r-3}\psi_z, \tag{70}$$

wherein the requirements of ψ_x, ψ_y, and ψ_z are given in (49)–(51). The finite element space is given by $DS_r(E) = \mathbb{P}_r(E) \oplus \mathbb{S}_r^{DS}(E)$, where

$$\mathbb{S}_r^{DS}(E) = \operatorname{span}\{\phi^f_{x,s},\ \phi^f_{y,s},\ \phi^f_{z,s},\ \phi^e_{x,\ell},\ \phi^e_{y,\ell},\ \phi^e_{z,\ell} \mid s = 0, 1, \dots, r-4,\ \ell = 1, 2, 3, 4\}. \tag{71}$$

Similar to the $r = 3$ case, $\phi^e_{x,m}$, $\phi^e_{y,m}$, and $\phi^e_{z,m}$ with $m = 1, 2, 3$ are used for the construction of the highest degree edge basis functions, and $\phi^e_{x,4}$, $\phi^e_{y,4}$, and $\phi^e_{z,4}$ are used for the construction of the second highest degree edge basis functions. The restriction of $\phi^e_{x,4}$, $\phi^e_{y,4}$, and $\phi^e_{z,4}$ on each face f_n belongs to $DS_r^{(2)}(f_n)$ (see (40)–(42)). Moreover,

$$\phi^e_{x,4}|_{e_{2,3}} = \lambda_{-1}\lambda_1\lambda_x^{r-3}, \quad \phi^e_{y,4}|_{e_{1,3}} = \lambda_{-2}\lambda_2\lambda_y^{r-3}, \quad \phi^e_{z,4}|_{e_{1,2}} = \lambda_{-3}\lambda_3\lambda_z^{r-3} \tag{72}$$

are zero on the faces that do not contain $e_{2,3}$, $e_{1,3}$, and $e_{1,2}$ as an edge, respectively.

In the rest of this section, we construct basis functions with respect to DoFs on each geometry object (i.e., vertex, edge, face, interior element) and conclude unisolvence of the DoFs.

5.1. Vertex and interior basis functions requiring no supplements

We take vertex basis functions $\phi^{\mathbf{v}}_{i,j,k}$, where $i = \pm 1$, $j = \pm 2$, and $k = \pm 3$, the same as given in (39), since these are 1 at $\mathbf{v}_{i,j,k}$, and 0 at all the other vertices. For $r \geq 6$, define interior element basis functions as $\phi^E_{s_1,s_2,s_3}$ with $0 \leq s_1 + s_2 + s_3 \leq r-6$ by

$$\phi^E_{s_1,s_2,s_3} = \Big(\prod_{n=-3}^{3} \lambda_n\Big)\lambda_x^{s_1}\lambda_y^{s_2}\lambda_z^{s_3}. \tag{73}$$

Such functions are zero on ∂E.

Lemma 5.1. *For any linear combination*

$$\phi = \sum_{0 \leq s_1+s_2+s_3 \leq r-6} c^E_{s_1,s_2,s_3}\phi^E_{s_1,s_2,s_3}, \tag{74}$$

if the interior DoFs defined in (29) vanish, then $\phi = 0$.

Proof. In (29), let

$$q = \sum_{0\le s_1+s_2+s_3\le r-6} c^E_{s_1,s_2,s_3} \lambda_x^{s_1}\lambda_y^{s_2}\lambda_z^{s_3} \in \mathbb{P}_{r-6}. \tag{75}$$

Then

$$\begin{aligned} 0 &= \int_E \phi \Big(\sum_{0\le s_1+s_2+s_3\le r-6} c^E_{s_1,s_2,s_3} \lambda_x^{s_1}\lambda_y^{s_2}\lambda_z^{s_3} \Big) \\ &= \int_E \Big(\prod_{n=-3}^{3} \lambda_n \Big) \Big(\sum_{0\le s_1+s_2+s_3\le r-6} c^E_{s_1,s_2,s_3} \lambda_x^{s_1}\lambda_y^{s_2}\lambda_z^{s_3} \Big)^2 \end{aligned} \tag{76}$$

implies that all the coefficients $c^E_{s_1,s_2,s_3}$ vanish by the non-negativity of the integrand and Lemma 2.1. □

5.2. Face basis functions

We next construct basis functions associated to the face DoFs (28). As an example, we want $\phi^f_{1;s_1,s_2}$ for face f_1 when $r \ge 4$, where $s_1 + s_2 \le r-4$, and, on the faces,

$$\phi^f_{1;s_1,s_2} = \begin{cases} \lambda_{-2}\lambda_2\lambda_{-3}\lambda_3\lambda_y^{s_1}\lambda_z^{s_2}, & \text{on } f_1, \\ 0, & \text{on } f_n, \quad n \ne 1. \end{cases} \tag{77}$$

We start the construction from the highest order. For $s_1 + s_2 = r-4$, we directly have from the supplement ϕ^f_{x,s_1} in (64) that

$$\begin{aligned} \phi^f_{1;s_1,s_2} &= \frac{1}{2}(\phi^f_{x,s_1} + \lambda_{-2}\lambda_2\lambda_{-3}\lambda_3\lambda_y^{s_1}\lambda_z^{s_2}) \\ &= \frac{1}{2}\lambda_{-2}\lambda_2\lambda_{-3}\lambda_3(1+R_x)\lambda_y^{s_1}\lambda_z^{s_2} \in \mathcal{D}S_r(E). \end{aligned} \tag{78}$$

We obtain the basis functions for lower order by induction. For any $0 \le s_0 \le r-5$, if we already have $\phi^f_{1;s_1',s_2'}$ for $s_1' + s_2' > s_0$, then we construct $\phi^f_{1;s_1,s_2}$ with $s_1 + s_2 = s_0$, from

$$\varphi^f_{1;s_1,s_2} = \lambda_{-1}\lambda_{-2}\lambda_2\lambda_{-3}\lambda_3\lambda_y^{s_1}\lambda_z^{s_2} \in \mathbb{P}_r(E). \tag{79}$$

It is zero on all the faces except f_1, where, using Lemma 2.3,

$$\varphi^f_{1;s_1,s_2}|_{f_1} = \lambda_{-2}\lambda_2\lambda_{-3}\lambda_3\lambda_y^{s_1}\lambda_z^{s_2}\big(A^1_{-1,yz} + B^1_{-1,yz}\lambda_y + C^1_{-1,yz}\lambda_z\big)\Big|_{f_1}. \tag{80}$$

By canceling the higher order terms in $\varphi^f_{1;s_1,s_2}$, we obtain the basis function

$$\phi^f_{1;s_1,s_2} = \frac{1}{A^1_{-1,yz}}\big(\varphi^f_{1;s_1,s_2} - B^1_{-1,yz}\phi^f_{1;s_1+1,s_2} - C^1_{-1,yz}\phi^f_{1;s_1,s_2+1}\big). \tag{81}$$

Note that although higher order terms are canceled here, it is not a necessary procedure, which means $\varphi^f_{1;s_1,s_2}$ are also able to serve as basis functions.

A similar construction gives ϕ^f_{n,s_1,s_2} for $n = -1, \pm 2, \pm 3$ and $0 \le s_1 + s_2 \le r-4$. We obtain $3(r-2)(r-3) = 6\dim\mathbb{P}_{r-4}(f)$ functions.

Lemma 5.2. *On any face f_n, suppose $\phi|_{f_n}$ can be represented as*

$$\phi|_{f_n} = \sum_{0\le s_1+s_2\le r-4} c^f_{n;s_1,s_2}\phi^f_{n;s_1,s_2}. \tag{82}$$

If the face DoFs for f_n defined in (28) vanish for ϕ, then $\phi|_{f_n} = 0$.

Proof. If the face DoFs (28) vanish for f_1, for example, in (28), let

$$q = \sum_{0\le s_1+s_2\le r-4} c^f_{1;s_1,s_2}\lambda_y^{s_1}\lambda_z^{s_2}. \tag{83}$$

Then (77) implies that the integrand is always non-negative on f_1 and the second part of Lemma 2.1 implies that all the coefficients $c^f_{1;s_1,s_2}$ vanish. By symmetry, we conclude that $c^f_{n;s_1,s_2} = 0$ for all $-3 \le n \le 3$ and $0 \le s_1 + s_2 \le r-4$. □

5.3. Edge basis functions

For illustration purpose, we construct $\phi^e_{i,j;s}$ for $i=\pm1$, $j=\pm2$, and $s=0,1,2,\dots,r-2$, such that on edges and faces,

$$\phi^e_{i,j;s} = \begin{cases} \lambda_{-3}\lambda_3\lambda_z^s, & \text{on } e_{i,j}. \\ 0, & \text{on } f_n, \quad n\neq i,j. \end{cases} \tag{84}$$

We start from the highest order $s=r-2$, where

$$\phi^e_{i,j;r-2} = \frac{1}{4}\lambda_{-3}\lambda_3\lambda_z^{r-2}(1+\operatorname{sign}(i)\,R_x)(1+\operatorname{sign}(j)\,R_y) \in DS_r(E), \tag{85}$$

using the supplements $\phi^e_{z,1}$, $\phi^e_{z,2}$, and $\phi^e_{z,3}$ in (67)–(69).

For $s=r-3$, the construction follows the idea of constructing $\phi^e_{i,j;0}$ for $DS_3(E)$ in Section 4.4, except for that they are multiplied through by λ_z^{r-3}. First of all, we directly have $\phi^e_{1,2;r-3}=\phi^e_{z,4}$ from (70). By the same procedure of finding proper linear combinations, using Lemma 2.2, we derive the basis functions

$$\begin{aligned} \phi^e_{-1,2;r-3} = \frac{1}{A^{-1,2}_{-2,z}}\Big(&\lambda_{-3}\lambda_3\lambda_z^{r-3}\lambda_{-2} - A^{1,2}_{-2,z}\phi^e_{z,4} \\ &- B^{1,2}_{-2,z}\phi^e_{1,2;r-2} - B^{-1,2}_{-2,z}\phi^e_{-1,2;r-2}\Big), \end{aligned} \tag{86}$$

$$\begin{aligned} \phi^e_{1,-2;r-3} = \frac{1}{A^{1,-2}_{-1,z}}\Big(&\lambda_{-3}\lambda_3\lambda_z^{r-3}\lambda_{-1} - A^{1,2}_{-1,z}\phi^e_{z,4} \\ &- B^{1,2}_{-1,z}\phi^e_{1,2;r-2} - B^{1,-2}_{-1,z}\phi^e_{1,-2;r-2}\Big). \end{aligned} \tag{87}$$

Finally, we directly obtain the basis function of order $s=r-3$ for $e_{-1,-2}$ by

$$\phi^e_{-1,-2;r-3} = \lambda_{-3}\lambda_3\lambda_z^{r-3} - \phi^e_{1,2;r-3} - \phi^e_{-1,2;r-3} - \phi^e_{1,-2;r-3}. \tag{88}$$

These functions are uniquely defined up to their values in the interior, no matter from which edge we start the construction.

We continue to construct basis functions for smaller s by induction. If we already have $\phi^e_{i,j;s}$ for $s>s_0$, where $0\le s_0\le r-4$, then we first construct

$$\varphi^e_{i,j;s_0} = \lambda_{-3}\lambda_3\lambda_{-i}\lambda_{-j}\lambda_z^{s_0} \in \mathbb{P}_r(E). \tag{89}$$

Note that

$$\varphi^e_{i,j;s_0} = \begin{cases} \lambda_{-3}\lambda_3\lambda_z^{s_0}(A^{i,j}_{-i,z}+B^{i,j}_{-i,z}\lambda_z)(A^{i,j}_{-j,z}+B^{i,j}_{-j,z}\lambda_z), & \text{on } e_{i,j}, \\ 0, & \text{on } f_n, \quad n\neq i,j. \end{cases} \tag{90}$$

Then we subtract higher order terms from it and get

$$\begin{aligned} \phi^e_{i,j;s_0} = \frac{1}{A^{i,j}_{-i,z}A^{i,j}_{-j,z}}\Big[&\varphi^e_{i,j;s_0} \\ &-(A^{i,j}_{-i,z}B^{i,j}_{-j,z}+A^{i,j}_{-j,z}B^{i,j}_{-i,z})\phi^e_{i,j;s_0+1} - B^{i,j}_{-i,z}B^{i,j}_{-j,z}\phi^e_{i,j;s_0+2}\Big]. \end{aligned} \tag{91}$$

If we want to simplify the construction, we can directly use $\varphi^e_{i,j;s_0}$ as the basis function of order s_0 on $e_{i,j}$ for $s_0\le r-4$. The basis construction for $e_{\pm1,\pm2}$ can be easily generalized to $e_{\pm1,\pm3}$ and $e_{\pm2,\pm3}$ by symmetry. We have constructed $12(r-1)=12\dim\mathbb{P}_{r-2}(e)$ functions.

Lemma 5.3. *On any edge $e_{m,n}$, suppose $\phi|_{e_{m,n}}$ could be represented as*

$$\phi|_{e_{m,n}} = \sum_{s=0}^{r-2} c^e_{m,n;s}\phi^e_{m,n;s}. \tag{92}$$

If the edge DoFs for $e_{m,n}$ defined in (27) vanish for ϕ, then $\phi|_{e_{m,n}}=0$.

Proof. We prove the argument for $m=\pm1$ and $n=\pm2$ as an example. If the edge DoFs (27) vanish, let

$$q = \sum_{s=0}^{r-2} c^e_{m,n;s}\lambda_z^s. \tag{93}$$

Since the integral is zero and the integrand is always non-negative on $e_{m,n}$ by (84), we conclude $c^e_{m,n;s}=0$ for all $s=0,1,\dots,r-2$ by the first part of Lemma 2.1. □

5.4. Unisolvence of the degrees of freedom

Lemma 2.1 gives certain polynomial bases for each geometry object (i.e., vertices, edges, faces, and interior element). We state and prove the unisolvence of DoFs in the following theorem.

Theorem 5.1. *The finite element $DS_r(E) = \mathbb{P}_r(E) \oplus \mathbb{S}_r^{DS}(E)$ with the basis functions of $\mathbb{S}_r^{DS}(E)$ defined by (64)–(70) is well-defined (i.e., unisolvent) with DoFs (26)–(29).*

Proof. Write $\phi \in DS_r(E)$ as

$$\begin{aligned}\phi = &\sum_{i=\pm1,j=\pm2,k=\pm3} c^{\mathbf{v}}_{i,j,k}\phi^{\mathbf{v}}_{i,j,k} \\ &+ \sum_{s=0}^{r-2}\Big(\sum_{j=\pm2,k=\pm3} c^{e}_{j,k;s}\phi^{e}_{j,k;s} + \sum_{i=\pm1,k=\pm3} c^{e}_{i,k;s}\phi^{e}_{i,k;s} + \sum_{i=\pm1,j=\pm2} c^{e}_{i,j;s}\phi^{e}_{i,j;s}\Big) \\ &+ \sum_{0\le s_1+s_2\le r-4}\sum_{n=-3}^{3} c^{f}_{n;s_1,s_2}\phi^{f}_{n;s_1,s_2} + \sum_{0\le s_1+s_2+s_3\le r-6} c^{E}_{s_1,s_2,s_3}\phi^{E}_{s_1,s_2,s_3}.\end{aligned} \tag{94}$$

Restricted to any vertex $\mathbf{v}_{i,j,k}$, only $\phi^{\mathbf{v}}_{i,j,k}$ is nonzero among all the basis functions. Therefore, if vertex DoFs (26) vanish for ϕ, we must have $c^{\mathbf{v}}_{i,j,k} = 0$ for all $i = \pm1, j = \pm2, k = \pm3$. Since $c^{\mathbf{v}}_{i,j,k} = 0$, and all the face and interior element basis functions are zero on edges, we have

$$\phi|_{e_{j,k}} = \sum_{s=0}^{r-2} c^{e}_{j,k;s}\phi^{e}_{j,k;s}, \quad \phi|_{e_{i,k}} = \sum_{s=0}^{r-2} c^{e}_{i,k;s}\phi^{e}_{i,k;s}, \quad \phi|_{e_{i,j}} = \sum_{s=0}^{r-2} c^{e}_{i,j;s}\phi^{e}_{i,j;s}, \tag{95}$$

for any edge $e_{j,k}$, $e_{i,k}$, and $e_{i,j}$. By Lemma 5.3, $c^{e}_{j,k;s} = c^{e}_{i,k;s} = c^{e}_{i,j;s} = 0$ for all the edges and $s = 0, 1, \dots, r-2$. Similarly, since all the vertex and edge coefficients are zero, and interior element basis functions vanish on faces, we have

$$\phi|_{f_n} = \sum_{0\le s_1+s_2\le r-4} c^{f}_{n;s_1,s_2}\phi^{f}_{n;s_1,s_2} \tag{96}$$

for all the faces f_n. By Lemma 5.2, $c^{f}_{n;s_1,s_2} = 0$ for all the faces f_n and $0 \le s_1 + s_2 \le r-4$. Since all the other coefficients vanish, we have ϕ consisting only of interior element basis functions. By Lemma 5.1, we finally conclude that all the coefficients vanish. □

6. Direct serendipity finite elements for $r \le 2$

We construct direct serendipity finite elements $DS_r(E)$ for $r = 1, 2$ as a subspace of $DS_3(E)$, which has been constructed explicitly in Section 4. The DoFs can be chosen either as defined in (26)–(27) or nodal DoFs.

For $i = \pm1, j = \pm2$, and $k = \pm3$, define $\phi^{\mathbf{v},\mathrm{low}}_{i,j,k} \in DS_3(E)$ for each vertex $\mathbf{v}_{i,j,k}$, such that it is linear on each edge, and is one at $\mathbf{v}_{i,j,k}$ while zero on all other vertices. These functions are uniquely defined in $DS_3(E)$, since there are no face or interior DoFs for $r = 3$. Furthermore, denote the edge basis functions $\phi^{e}_{j,k;0}$, $\phi^{e}_{i,k;0}$, and $\phi^{e}_{i,j;0}$ defined for $DS_3(E)$ as $\phi^{e,\mathrm{low}}_{j,k}$, $\phi^{e,\mathrm{low}}_{i,k}$, and $\phi^{e,\mathrm{low}}_{i,j}$, respectively. Define

$$DS_1(E) = \mathrm{span}\{\phi^{\mathbf{v},\mathrm{low}}_{i,j,k} \mid i = \pm1,\ j = \pm2,\ k = \pm3\}, \tag{97}$$

$$\begin{aligned}DS_2(E) = DS_1(E) \oplus \mathrm{span}\{&\phi^{e,\mathrm{low}}_{j,k}, \phi^{e,\mathrm{low}}_{i,k}, \phi^{e,\mathrm{low}}_{i,j} \\ &\mid i = \pm1,\ j = \pm2,\ k = \pm3\}.\end{aligned} \tag{98}$$

Theorem 6.1. *For $r = 1, 2$, the lower order spaces $DS_r(E)$ defined as (97)–(98) satisfy that $\mathbb{P}_r(E) \subset DS_r(E)$.*

Proof. For any $p \in \mathbb{P}_r(E)$, there is a unique function $\phi \in DS_r(E)$ having the same evaluation of DoFs as p. Moreover, restricted to any edge $e_{m,n}$, $\phi|_{e_{m,n}}$ has to be a polynomial of order r by construction (97)–(98). Any function in $DS_3(E)$ is uniquely defined by its shape on edges and vertices. Since we both have $p \in DS_3(E)$ and $\phi \in DS_3(E)$ with the same values restricted to edges and vertices, we must have $p = \phi$. □

More details on the construction of $DS_1(E)$ are now given. The special functions R_x, R_y, R_z, ψ_x, ψ_y, and ψ_z must be constructed beforehand (see Section 7). These are used to define the space $DS_3(E)$. Specifically, one needs the edge functions $\phi^{e}_{i,j;1}$, defined in (43)–(45), and the edge functions $\phi^{e}_{i,j;0}$, defined in (52) and Section 4.4. For $i = \pm1$, $j = \pm2$, and $k = \pm3$, the vertex basis function $\phi^{\mathbf{v},\mathrm{low}}_{i,j,k}$ is the linear combination

$$\begin{aligned}\phi^{\mathbf{v},\mathrm{low}}_{i,j,k} = &\phi^{\mathbf{v}}_{i,j,k} + \alpha_0\phi^{e}_{i,j;0} + \alpha_1\phi^{e}_{i,j;1} + \beta_0\phi^{e}_{i,k;0} + \beta_1\phi^{e}_{i,k;1} \\ &+ \gamma_0\phi^{e}_{j,k;0} + \gamma_1\phi^{e}_{j,k;1},\end{aligned} \tag{99}$$

for some coefficients α_0, α_1, β_0, β_1, γ_0, and γ_1, where $\phi^{\mathbf{v}}_{i,j,k}$ is defined in (39). Note that $\phi^{\mathbf{v},\mathrm{low}}_{i,j,k}$ is zero on faces f_{-i}, f_{-j}, and f_{-k}, and zero at each vertex save $\mathbf{v}_{i,j,k}$, where it is one. However, $\phi^{\mathbf{v},\mathrm{low}}_{i,j,k}$ is in general cubic on each edge emanating from $\mathbf{v}_{i,j,k}$. The coefficients

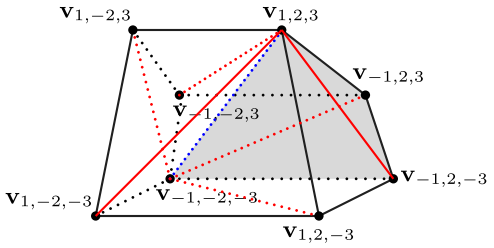

Fig. 3. The partition of marching tetrahedra $\mathcal{T}_E^M$, where $T_{2,-1}^M$ is painted in gray.

are chosen to ensure that $\phi_{i,j,k}^{\mathbf{v},\mathrm{low}}$ is linear on these edges. For example, consider $\phi_{1,2,3}^{\mathbf{v},\mathrm{low}}$ and the edge $e_{2,3}$ from $\mathbf{v}_{1,2,3}$ to $\mathbf{v}_{-1,2,3}$. Divide the edge into thirds at the points $\mathbf{x}_{2,3}^+$ (nearer to $\mathbf{v}_{1,2,3}$) and $\mathbf{x}_{2,3}^-$. Then one must solve the linear system

$$\begin{pmatrix} \phi_{2,3;0}^e(\mathbf{x}_{2,3}^+) & \phi_{2,3;1}^e(\mathbf{x}_{2,3}^+) \\ \phi_{2,3;0}^e(\mathbf{x}_{2,3}^-) & \phi_{2,3;1}^e(\mathbf{x}_{2,3}^-) \end{pmatrix} \begin{pmatrix} \gamma_0 \\ \gamma_1 \end{pmatrix} = \begin{pmatrix} \frac{2}{3} - \phi_{1,2,3}^{\mathbf{v}}(\mathbf{x}_{2,3}^+) \\ \frac{1}{3} - \phi_{1,2,3}^{\mathbf{v}}(\mathbf{x}_{2,3}^-) \end{pmatrix}. \tag{100}$$

7. Construction of the special functions R_* and ψ_*

We present two ways of filling in the interior of the needed special functions. Recall that the boundary values required of R_x, R_y, and R_z are specified in (7), and those of ψ_x, ψ_y, and ψ_z are found in (49)–(51). The first way results in smooth supplemental functions, while the second way constructs supplements that are piecewise polynomials in $H^1(E)$.

7.1. Smooth supplemental functions

The first construction makes use of the mapping $\mathbf{x} = \mathbf{F}_E(\hat{\mathbf{x}})$ from a reference element $\hat{E}$ introduced in Section 2. With $\hat{\mathbf{x}} = \mathbf{F}_E^{-1}(\mathbf{x}) = (\hat{x}, \hat{y}, \hat{z})$, we define ψ_x, ψ_y, and ψ_z on the element E by

$$\psi_x(\mathbf{x}) = \hat{\psi}_x(\hat{\mathbf{x}}) = \hat{\psi}_x(\hat{x}, \hat{y}, \hat{z}) = \psi_{x,2}(\mathbf{F}_E(\hat{x}, 1, \hat{z}))\, \psi_{x,3}(\mathbf{F}_E(\hat{x}, \hat{y}, 1)), \tag{101}$$

$$\psi_y(\mathbf{x}) = \hat{\psi}_y(\hat{\mathbf{x}}) = \hat{\psi}_y(\hat{x}, \hat{y}, \hat{z}) = \psi_{y,1}(\mathbf{F}_E(1, \hat{y}, \hat{z}))\, \psi_{y,3}(\mathbf{F}_E(\hat{x}, \hat{y}, 1)), \tag{102}$$

$$\psi_z(\mathbf{x}) = \hat{\psi}_z(\hat{\mathbf{x}}) = \hat{\psi}_z(\hat{x}, \hat{y}, \hat{z}) = \psi_{z,1}(\mathbf{F}_E(1, \hat{y}, \hat{z}))\, \psi_{z,2}(\mathbf{F}_E(\hat{x}, 1, \hat{z})), \tag{103}$$

where $\psi_{x,2}, \dots, \psi_{z,2}$ are defined in (49)–(51). It is not difficult to verify that these functions have the required properties. Moreover, they are smooth if $R_x|_{f_2}$, $R_x|_{f_3}$, $R_y|_{f_1}$, $R_y|_{f_3}$, $R_z|_{f_1}$ and $R_z|_{f_2}$ are smooth. For example, R_x, R_y, and R_z could be taken as in (8).

7.2. H^1 supplemental functions

The second construction makes use of partitions of the hexahedron into tetrahedra, of which two partitions are discussed.

We first consider a partition based on marching tetrahedra, as discussed in [23], where the element E is divided into six tetrahedra as shown in Fig. 3. An interior diagonal mesh line joining vertex $\mathbf{v}_{-1,-2,-3}$ to $\mathbf{v}_{1,2,3}$ is added, as well as six mesh lines on the faces joining $\mathbf{v}_{\pm1,-2,-3}$ to $\mathbf{v}_{\pm1,2,3}$, $\mathbf{v}_{-1,\pm2,-3}$ to $\mathbf{v}_{1,\pm2,3}$, and $\mathbf{v}_{-1,-2,\pm3}$ to $\mathbf{v}_{1,2,\pm3}$. Denote this sub-partition as $\mathcal{T}_E^M$ and the tetrahedron which has two faces lying in f_m and f_n as $T_{m,n}^M$. We remark that this partition naturally matches adjacent hexahedra in a logically rectangular mesh.

Let the piecewise continuous polynomial spaces corresponding to the partition be denoted

$$\mathcal{P}_s(\mathcal{T}_E^M) = \left\{ f \in C^0(E) \ : \ f|_{T_{m,n}^M} \in \mathbb{P}_s(T_{m,n}^M)\ \forall m, n \right\}. \tag{104}$$

Define R_x, R_y, and R_z in $\mathcal{P}_1(\mathcal{T}_E^M)$ according to (7) by fixing each vertex value to be either -1 or 1.

Since the functions R_* are piecewise linear, the functions ψ_x, ψ_y, and ψ_z satisfying (49)–(51) must be piecewise continuous quadratic functions. They can be defined in $\mathcal{P}_2(\mathcal{T}_E^M)$ by interpolation at the vertices and mesh line midpoints of the sub-partition. However, each of these functions is fixed only on four of the faces of E, and so no values are given at the midpoints of three sub-partition mesh lines (two lying on faces, one being the interior diagonal line). We need to fix these values to define ψ_x, ψ_y, and ψ_z, and any value will suffice (such as taking the average of the ends at the midpoint). By such a construction, all the supplemental functions will be piecewise polynomials that are continuous on E, so they will lie in $H^1(E)$.

The second partition is based on the diamond lattice cells, which divides the hexahedron E into five tetrahedra with exactly one having all its faces in the interior of E. The partition uses six additional mesh lines that all lie in ∂E. As shown in Fig. 4, there are two patterns for this partition. First, one can take the "even" set of vertices $\mathbf{v}_{1,2,3}$, $\mathbf{v}_{-1,-2,3}$, $\mathbf{v}_{-1,2,-3}$, and $\mathbf{v}_{1,-2,-3}$, and the six mesh lines joining each pair. Denote this pattern as $\mathcal{T}_E^D$. Second, one can take the "odd" set of vertices $\mathbf{v}_{-1,-2,-3}$, $\mathbf{v}_{-1,2,3}$, $\mathbf{v}_{1,-2,3}$, and $\mathbf{v}_{1,2,-3}$,

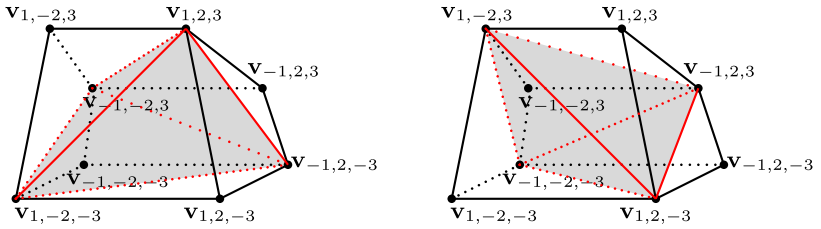

Fig. 4. The diamond cubic based partition $\mathcal{T}_E^D$ (left) and $\mathcal{T}_E^{D'}$ (right). Displayed in gray for both partitions is the tetrahedron with all four faces internal to E.

and the six mesh lines joining each pair, to obtain the pattern denoted as $\mathcal{T}_E^{D'}$. We remark that these patterns appear alternately for adjacent hexahedra in a logically rectangular mesh.

Similar to the case for the marching tetrahedra, the special functions R_x, R_y, and R_z can be interpolated into $\mathcal{P}_1(\mathcal{T}_E^D)$ or $\mathcal{P}_1(\mathcal{T}_E^{D'})$. Moreover, ψ_x, ψ_y, and ψ_z, can be interpolated into $\mathcal{P}_2(\mathcal{T}_E^D)$ or $\mathcal{P}_2(\mathcal{T}_E^{D'})$. We will need to fix arbitrarily the midpoint values of the two mesh lines of the sub-partition not fixed by the required function values.

8. Defining an H^1-conforming space on the domain

Direct serendipity elements in 2D are not uniquely defined, as discussed in [16]. The traces of our 3D elements on the faces are affected by our choice of the functions R_x, R_y, and R_z and the functions λ_x, λ_y, and λ_z. When merging two elements together, these choices must be respected by the adjoining elements.

Consider two adjacent elements E_1 and E_{-1} joined on the face $f = E_1 \cap E_{-1}$. For simplicity of the discussion, we assume that in the notation of this paper, E_1 considers f as being its f_1, and E_{-1} considers f as being its f_{-1}. Moreover, we denote the special functions on f restricted to $E_{\pm 1}$ as being $R_{y,\pm 1}$, $R_{z,\pm 1}$, $\lambda_{y,\pm 1}$, and $\lambda_{z,\pm 1}$.

We must ask two things. First, we require that,

$$R_{\alpha,1}|_f = \pm R_{\alpha,-1}|_f, \quad \alpha = y, z. \tag{105}$$

We are dealing with vector spaces, so technically the two expressions need only be multiples of each other, but they are ± 1 on opposite edges. The constructions in Section 7 have this property. For the smooth case, the functions R_* are defined in (8) by the trilinear mapping of the reference cube to $E_{\pm 1}$. The trilinear map restricts to a bilinear map on each face, determined only by its four vertices. Therefore the value of $R_{\alpha,\pm 1}|_f$ must agree with the value of $\hat{\alpha}$, $\alpha = y, z$, up to its sign. For the H^1 supplemental function case, we merely ask that the partition of neighboring elements coincide when restricted to the common face. In the case of a logically rectangular mesh, this is satisfied naturally by marching tetrahedra. However, if we use the partition based on diamond lattice cells, two neighboring elements that share a common face must use different patterns $\mathcal{T}_E^D$ and $\mathcal{T}_E^{D'}$ to match.

Second, we must ask that the special linear functions agree up to a multiple. That is, the zero line of $\lambda_{\alpha,\pm 1}|_f$ is denoted $\mathcal{P}_{\alpha,\pm 1} \cap f$, and we require that

$$\mathcal{P}_{\alpha,1} \cap f = \mathcal{P}_{\alpha,-1} \cap f, \quad \alpha = y, z. \tag{106}$$

This requirement is more delicate to enforce on a general mesh. To illustrate a very special case, suppose that our mesh is composed only of elements that have consistent mid planes, meaning that the midpoints of the four edges $e_{\pm 1,\pm 2}$ form a plane, and similarly for $e_{\pm 1,\pm 3}$ and $e_{\pm 2,\pm 3}$. We could then simply take these three planes as the zero planes of our three special linear functions. But the consistent mid plane condition is a severe restriction on the mesh.

We can resolve the issue if we restrict to the most natural situation of a logically rectangular mesh. In that case, a simple choice is to take

$$\lambda_x = \lambda_{-1}, \quad \lambda_y = \lambda_{-2}, \quad \lambda_z = \lambda_{-3}. \tag{107}$$

The zero lines on the faces then agree between pairs of elements, so the condition (106) is satisfied.

9. Approximation results

We give a summary of the necessary constructions and the main approximation results without complete proofs, since the development closely follows that for direct serendipity finite elements on quadrilaterals discussed in [16]. A minor issue is that [16] assumes extra smoothness of the special functions analogous to those in (7), but this extra smoothness requirement was removed in [24,25], allowing only piecewise continuous, differentiable functions. The uniform shape regularity of the mesh $\mathcal{T}_h$ on the domain Ω is assumed for the purpose of proving global approximation properties, with its definition generalized from [26, pp. 104–105].

Definition 9.1. For any $E \in \mathcal{T}_h$, denote by $T_{i,j,k}$, $i = \pm 1$, $j = \pm 2$, $k = \pm 3$, the sub-tetrahedron of E with vertices $\mathbf{v}_{i,j,k}$, $\mathbf{v}_{-i,j,k}$, $\mathbf{v}_{i,-j,k}$, and $\mathbf{v}_{i,j,-k}$ of E. Define the parameters

$$h_E = \text{diameter of } E, \tag{108}$$

$$\rho_E = \min_{i,j,k}\{\text{diameter of the largest sphere inscribed in } T_{i,j,k}\}. \tag{109}$$

A collection of meshes $\{\mathcal{T}_h\}_{h>0}$ is *uniformly shape regular* if there exists a *shape regularity parameter* $\sigma_* > 0$, independent of $\mathcal{T}_h$ and $h > 0$, such that the ratio

$$\frac{\rho_E}{h_E} \ge \sigma_* > 0 \quad \text{for all } E \in \mathcal{T}_h. \tag{110}$$

We construct an interpolation operator that maps onto $\mathcal{DS}_r$ inspired by Scott and Zhang [27]. For the purpose of the proof, denote the global nodal points as $\{a_1, \dots, a_{N_r}\}$ with $N_r = \dim \mathcal{DS}_r$. For each nodal point a_i, denote its corresponding global nodal basis function as φ_i. We require that the nodal points on an element depend continuously on its vertices. If a_i lies in the interior cell of an element $E \in \mathcal{T}_h$, we set K_i to be (the closed set) E. These are referred to as *interior* nodes. If a_i lies in the interior of face f of $\mathcal{T}_h$ (i.e., not on the edges or at the vertices), we set $K_i = f$ (a closed set), and a_i is referred to as a *face* node. If a_i belongs to the interior of an edge or is a vertex of $\mathcal{T}_h$, K_i is chosen to be any fixed face f containing a_i, with the additional requirement that if $a_i \in \partial\Omega$, then $f \subset \partial\Omega$. Those nodes are said to be *edge* and *vertex* nodes, respectively. Note that for such nodes, we are free to chose f from among multiple faces.

An L^2-dual nodal basis, denoted as $\{\psi_1, \dots, \psi_{N_r}\}$, is defined as follows. Firstly, let n_i be the total number of nodes in K_i. Secondly, denote the nodes in K_i as $\{a_{i,j} : j = 1, \dots, n_i\}$ with $a_{i,1} = a_i$, corresponding to the global nodal basis functions $S_i = \{\varphi_{i,j} : j = 1, \dots, n_i\}$. Thirdly, define an $L^2(K_i)$-dual nodal basis $\{\psi_{i,j} : j = 1, \dots, n_i\} \subset \operatorname{span} S_i$ satisfying

$$\int_{K_i} \psi_{i,j}(\mathbf{x})\, \varphi_{i,k}(\mathbf{x})\, d\mathbf{x} = \delta_{jk}, \quad j,k = 1,2,\dots,n_i, \tag{111}$$

where we use a slight abuse of notation in that $d\mathbf{x}$ should be $d\sigma(x)$ when K_i is a face. Finally, for the node a_i, its corresponding L^2-dual nodal basis function is taken to be $\psi_i = \psi_{i,1}$. For each node a_i giving rise to K_i and ψ_i, we can prove that

$$\int_{K_i} \psi_i(\mathbf{x})\, \varphi_j(\mathbf{x})\, d\mathbf{x} = \delta_{ij}, \quad i,j = 1,2,\dots,N_r. \tag{112}$$

We define an interpolation operator $\mathcal{I}_h^r : W_p^l(\Omega) \to \mathcal{DS}_r$ by

$$\mathcal{I}_h^r v(\mathbf{x}) = \sum_{i=1}^{N_r} \varphi_i(\mathbf{x}) \int_{K_i} \psi_i(\mathbf{y})\, v(\mathbf{y})\, d\mathbf{y} \in \mathcal{DS}_r, \tag{113}$$

where $1 \le p \le \infty$ and $l > 1/p$ (but $l \ge 1$ if $p = 1$). Note that for any $v \in W_p^l(\Omega)$, the nodal values $\int_{K_i} \psi_i(\mathbf{y})\, v(\mathbf{y})\, d\mathbf{y}$ are well defined according to the trace theorem. With a proof analogous to [16,24,25], we can derive the following lemma by a continuity and compactness argument.

Lemma 9.1. *Let $v \in W_p^l(\Omega)$, where $1 \le p \le \infty$ and $\ell > 1/p$ (or $\ell \ge 1$ if $p = 1$). Let $\mathcal{T}_h$ be uniformly shape regular (Definition 9.1) with shape regularity parameter σ_*. For every $E \in \mathcal{T}_h$, suppose that $\mathcal{DS}_r(E)$ are constructed with λ_x, λ_y, and λ_z such that the intersection of their zero set depends on the vertices of E continuously. Moreover, assume that R_x, R_y, R_z, ψ_x, ψ_y, and ψ_z are piecewise uniformly differentiable $H^1(E)$ functions of the vertices of E up to order m. Then for $r \ge 1$, $E \in \mathcal{T}_h$, $1 \le q \le \infty$, and any nonnegative integer m,*

$$\|\mathcal{I}_h^r v\|_{W_q^m(E)} \le C(\sigma_*, m, q) \sum_{k=0}^{\ell} h_E^{k-m+\frac{3}{q}-\frac{3}{p}} |v|_{W_p^k(E^*)}, \tag{114}$$

where $E^* = \bigcup_{F \in \mathcal{T}_h,\, F \cap E \ne \emptyset} F$ and $|\cdot|_{W_p^k}$ is the seminorm of kth order derivatives.

Combining Lemma 9.1 and the Bramble–Hilbert lemma [28] in the form developed by Dupont and Scott in [29] leads to the following error estimation results.

Theorem 9.1. *With the assumptions of Lemma 9.1, there exists a constant $C = C(r, \sigma_*) > 0$ such that for all functions $v \in W_p^\ell(E^*)$, with $1 \le p \le \infty$ and $\ell > 1/p$ (or $\ell \ge 1$ if $p = 1$),*

$$\|v - \mathcal{I}_h^r v\|_{W_p^m(E)} \le C\, h_E^{\ell-m} |v|_{W_p^\ell(E^*)}, \quad 0 \le m \le \min(\ell, r+1). \tag{115}$$

Moreover, there exists a constant $C = C(r, \sigma_*) > 0$, independent of $h = \max_{E \in \mathcal{T}_h} h_E$, such that for all functions $v \in W_p^\ell(\Omega)$,

$$\Big(\sum_{E \in \mathcal{T}_h} \|v - \mathcal{I}_h^r v\|_{W_p^m(E)}^p \Big)^{1/p} \le C\, h^{\ell-m} |v|_{W_p^\ell(\Omega)}, \quad 0 \le m \le \min(\ell, r+1). \tag{116}$$

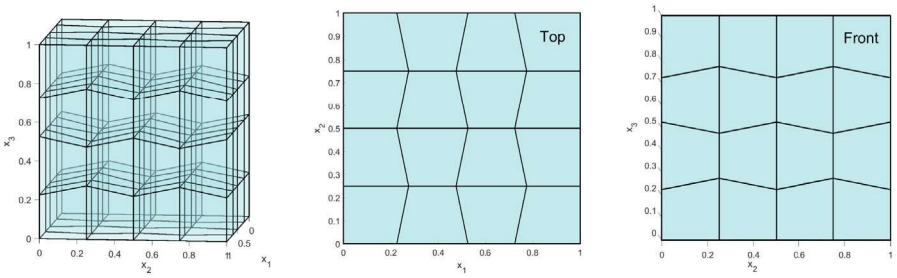

Fig. 5. Plots of the $\mathcal{T}_h^1$ mesh for $n = 4$ with a general view, a top view, and a front view.

10. Some numerical tests

We test the new finite elements using Poisson's equation

$$-\nabla\cdot(\nabla p) = f \quad \text{in } \Omega, \tag{117}$$

$$p = 0 \quad \text{on } \partial\Omega, \tag{118}$$

where $f \in L^2(\Omega)$. The problem can be written in the weak form: Find $p \in H_0^1(\Omega)$ such that

$$(\nabla p, \nabla q) = (f, q), \quad \forall q \in H_0^1(\Omega), \tag{119}$$

where $(\cdot,\cdot)$ is the $L^2(\Omega)$ inner product. In view of Theorem 9.1, it is well known that the following theorem holds [30].

Theorem 10.1. *Let $\mathcal{T}_h$ be uniformly shape regular with shape regularity parameter σ_* and let the assumption in Theorem 9.1 hold. There exists a constant $C > 0$, depending on r and σ_* but otherwise independent of $\mathcal{T}_h$ and $h > 0$, such that*

$$\|p - p_h\|_{H^m(\Omega)} \le C\, h^{s+1-m}\, |p|_{H^{s+1}(\Omega)}, \quad s = 0, 1, \dots, r, \quad m = 0, 1, \tag{120}$$

where $p_h \in \mathcal{DS}_r(\Omega) \cap H_0^1(\Omega)$ approximates the solution p of (119) for $r \ge 1$.

We consider the test problem (117)–(118) on the cubical domain $\Omega = [0,1]^3$. The analytical solution of the test problem is

$$p(x_1, x_2, x_3) = \sin(\pi x_1)\sin(\pi x_2)\sin(\pi x_3),$$

with the source term $f(x_1, x_2, x_3) = 3\pi^2 \sin(\pi x_1)\sin(\pi x_2)\sin(\pi x_3)$.

The numerical solutions are computed on two sequences of $n \times n \times n$ meshes for $n = 4, 8, 12, 16$. Let the global vertices be $\mathbf{v}_{i,j,k}^{\text{global}} = (x_{1;i,j,k}^{\text{global}}, x_{2;i,j,k}^{\text{global}}, x_{3;i,j,k}^{\text{global}})$ for $0 \le i, j, k \le n$. The first set of meshes, $\mathcal{T}_h^1$, is generated by deviating the interior vertices of a cubical mesh regularly such that there are two pairs of non-parallel faces in each element, with the vertices defined by

$$x_{1;i,j,k}^{\text{global}} = \begin{cases} \frac{1}{n}(i + 0.1), & \text{if} \quad i\%2 = j\%2 \quad \text{and} \quad 0 < i < n, \\ \frac{1}{n}(i - 0.1), & \text{if} \quad i\%2 \ne j\%2 \quad \text{and} \quad 0 < i < n, \\ \frac{i}{n}, & \text{if} \quad i = 0, n, \end{cases} \tag{121}$$

$$x_{2;i,j,k}^{\text{global}} = jh, \tag{122}$$

$$x_{3;i,j,k}^{\text{global}} = \begin{cases} \frac{1}{n}(k + 0.1), & \text{if} \quad k\%2 = j\%2 \quad \text{and} \quad 0 < k < n, \\ \frac{1}{n}(k - 0.1), & \text{if} \quad k\%2 \ne j\%2 \quad \text{and} \quad 0 < k < n, \\ \frac{k}{n}, & \text{if} \quad k = 0, n. \end{cases} \tag{123}$$

We show the $\mathcal{T}_h^1$ mesh for $n = 4$ as an example in Fig. 5.

The second set of meshes, $\mathcal{T}_h^2$, are generated randomly by first deviating the vertices on the lower boundaries $\{x_1 = 0\} \cup \{x_2 = 0\} \cup \{x_3 = 0\}$. For the distortion factor d and random numbers $r_{1;i,j,k}, r_{2;i,j,k}, r_{3;i,j,k}$ generated from uniform distribution $[-1, 1]$, define

$$x_{1;i,j,k}^{\text{global}} = \begin{cases} \frac{1}{n}(i + d\, r_{1;i,j,k}), & \text{if} \quad j = 0 \text{ or } k = 0, \quad \text{and} \quad 0 < i < n, \\ \frac{i}{n}, & \text{if} \quad j = 0 \text{ or } k = 0, \quad \text{and} \quad i = 0, n, \end{cases} \tag{124}$$

$$x_{2;i,j,k}^{\text{global}} = \begin{cases} \frac{1}{n}(j + d\, r_{2;i,j,k}), & \text{if} \quad i = 0 \text{ or } k = 0, \quad \text{and} \quad 0 < j < n, \\ \frac{j}{n}, & \text{if} \quad i = 0 \text{ or } k = 0, \quad \text{and} \quad j = 0, n, \end{cases} \tag{125}$$

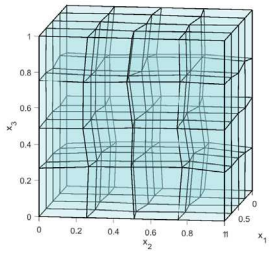

Fig. 6. A plot of the $\mathcal{T}_h^2$ mesh for $n = 4$ with a general view.

Table 2
Errors and convergence rates for DS_r^{S} on $\mathcal{T}_h^1$.

n	$r=1$		$r=2$		$r=3$		$r=4$	
	Error	Rate	Error	Rate	Error	Rate	Error	Rate
L^2 errors and convergence rates								
4	7.688e−02	–	5.453e−03	–	1.445e−03	–	1.882e−04	–
8	1.878e−02	2.03	6.935e−04	2.98	9.020e−05	4.00	5.843e−06	5.01
12	8.333e−03	2.00	2.065e−04	2.98	1.773e−05	4.01	7.698e−07	4.99
16	4.688e−03	2.00	8.730e−05	3.00	5.590e−06	4.02	1.830e−07	5.00
H^1-seminorm errors and convergence rates								
4	2.438e−01	–	2.778e−02	–	9.693e−03	–	1.362e−03	–
8	1.204e−01	1.02	6.739e−03	2.04	1.187e−03	3.03	8.555e−05	3.99
12	8.022e−02	1.00	2.985e−03	2.01	3.500e−04	3.01	1.693e−05	3.99
16	6.019e−02	1.00	1.678e−03	2.00	1.473e−04	3.01	5.372e−06	4.00

$$x_{3;i,j,k}^{\text{global}} = \begin{cases} \frac{1}{n}(k + d\, r_{3;i,j,k}), & \text{if} \quad i = 0 \text{ or } j = 0, \quad \text{and} \quad 0 < k < n, \\ \frac{k}{n}, & \text{if} \quad i = 0 \text{ or } j = 0, \quad \text{and} \quad k = 0, n. \end{cases} \tag{126}$$

For each hexahedral element, since all the faces are required to be flat, seven vertices are enough to decide the location of the eighth. Therefore, all the other vertices such that $i, j, k > 0$ are consequently decided by the order of ascending indices. However, by this definition, the irregularity of the element will increase for larger indices. For the same distortion factor d, the σ_* in Definition 9.1 can decrease for larger n. Therefore, we pick $d = 0.075, 0.063, 0.055, 0.056$ for $n = 4, 8, 12, 16$, respectively, such that σ_* is approximately 0.1 to three decimal precision. A plot of $\mathcal{T}_h^2$ mesh with $n = 4$ is shown in Fig. 6 as an example.

We present the convergence results for DS_r with $r = 1, 2, 3, 4$ on the meshes with $n = 4, 8, 12, 16$. The results are compared for three different definitions of supplemental functions. Denote the direct serendipity space with the smooth supplements, the piecewise polynomial supplements based on marching tetrahedra, and those based on diamond lattice cells as DS_r^{S}, DS_r^{M} and DS_r^{D}, respectively.

10.1. Shape regular meshes $\mathcal{T}_h^1$

The errors and the corresponding convergence rates of DS_r^{S} on $\mathcal{T}_h^1$ are presented in Table 2. The convergence rates are approximately $r+1$ for L^2-norm error, and r for H^1-seminorm error, which agree with Theorem 10.1. The errors and the convergence rates for DS_r^{M} and DS_r^{D} are shown in Tables 3 and 4. We note that the errors for DS_r^{M} and DS_r^{D} are slightly worse than those of DS_r^{S} for higher r. We suppose that this is because smooth supplements behave better in approximating smooth functions.

10.2. Randomly generated meshes $\mathcal{T}_h^2$

We show the errors and convergence rates for DS_r^{S}, DS_r^{M}, and DS_r^{D} on $\mathcal{T}_h^2$ in Tables 5–7. The results are similar to those of $\mathcal{T}_h^1$. For all the direct serendipity spaces, we observe optimal convergence rates, with the errors for DS_r^{S} being smaller than DS_r^{M} and DS_r^{D} for larger r.

11. Conclusions

We constructed direct serendipity finite elements on a general non-degenerate cuboidal hexahedron E, which is a three-dimensional polytope with all the faces being flat, and that can be obtained by some trilinear map of a cube. For approximation purposes, $DS_r(E)$ takes the form

$$DS_r(E) = \mathbb{P}_r(E) \oplus \mathbb{S}_r^{DS}(E), \quad r \geq 1, \tag{127}$$

Table 3
Errors and convergence rates for DS_r^{M} on $\mathcal{T}_h^1$.

n	$r=1$		$r=2$		$r=3$		$r=4$	
	Error	Rate	Error	Rate	Error	Rate	Error	Rate
L^2 errors and convergence rates								
4	7.682e−02	–	7.032e−03	–	5.219e−03	–	5.912e−04	–
8	1.879e−02	2.03	7.089e−04	3.31	2.410e−04	4.44	1.603e−05	5.20
12	8.339e−03	2.00	2.069e−04	3.03	4.433e−05	4.17	1.999e−06	5.13
16	4.691e−03	2.00	8.702e−05	3.01	1.362e−05	4.11	4.628e−07	5.09
H^1-seminorm errors and convergence rates								
4	2.437e−01	–	3.922e−02	–	3.070e−02	–	4.121e−03	–
8	1.204e−01	1.02	7.322e−03	2.42	3.436e−03	3.16	2.478e−04	4.06
12	8.023e−02	1.00	3.082e−03	2.13	9.825e−04	3.08	4.747e−05	4.07
16	6.020e−02	1.00	1.703e−03	2.06	4.080e−04	3.06	1.480e−05	4.06

Table 4
Errors and convergence rates for DS_r^{D} on $\mathcal{T}_h^1$.

n	$r=1$		$r=2$		$r=3$		$r=4$	
	Error	Rate	Error	Rate	Error	Rate	Error	Rate
L^2 errors and convergence rates								
4	7.691e−02	–	6.158e−03	–	3.747e−03	–	4.831e−04	–
8	1.873e−02	2.04	7.081e−04	3.12	2.281e−04	4.04	1.612e−05	4.91
12	8.302e−03	2.00	1.988e−04	3.13	4.498e−05	4.00	2.128e−06	4.99
16	4.669e−03	2.00	8.210e−05	3.08	1.421e−05	4.01	5.036e−07	5.02
H^1-seminorm errors and convergence rates								
4	2.440e−01	–	3.407e−02	–	2.589e−02	–	3.598e−03	–
8	1.202e−01	1.02	7.111e−03	2.26	3.197e−03	3.02	2.417e−04	3.90
12	8.010e−02	1.00	2.955e−03	2.16	9.419e−04	3.01	4.794e−05	3.99
16	6.009e−02	1.00	1.621e−03	2.09	3.963e−04	3.01	1.517e−05	4.01

Table 5
Errors and convergence rates for DS_r^{S} on $\mathcal{T}_h^2$.

n	$r=1$		$r=2$		$r=3$		$r=4$	
	Error	Rate	Error	Rate	Error	Rate	Error	Rate
L^2 errors and convergence rates								
4	7.508e−02	–	5.109e−03	–	1.317e−03	–	1.770e−04	–
8	1.797e−02	2.21	6.252e−04	3.24	7.446e−05	4.43	5.327e−06	5.40
12	7.626e−03	2.12	1.885e−04	2.96	1.342e−05	4.24	6.956e−07	5.03
16	4.349e−03	2.30	8.192e−05	3.41	4.406e−06	4.56	1.720e−07	5.73
H^1-seminorm errors and convergence rates								
4	2.410e−01	–	2.571e−02	–	9.244e−03	–	1.263e−03	–
8	1.181e−01	1.10	6.006e−03	2.24	1.092e−03	3.29	7.755e−05	4.30
12	7.697e−02	1.06	2.677e−03	2.00	3.031e−04	3.17	1.533e−05	4.01
16	5.788e−02	1.17	1.527e−03	2.30	1.307e−04	3.45	5.002e−06	4.59

Table 6
Errors and convergence rates for DS_r^{M} on $\mathcal{T}_h^2$.

n	$r=1$		$r=2$		$r=3$		$r=4$	
	Error	Rate	Error	Rate	Error	Rate	Error	Rate
L^2 errors and convergence rates								
4	7.510e−02	–	6.793e−03	–	5.130e−03	–	5.733e−04	–
8	1.797e−02	2.21	6.439e−04	3.63	2.240e−04	4.83	1.490e−05	5.63
12	7.627e−03	2.12	1.903e−04	3.01	4.116e−05	4.19	1.877e−06	5.12
16	4.349e−03	2.30	8.225e−05	3.44	1.283e−05	4.78	4.434e−07	5.91
H^1-seminorm errors and convergence rates								
4	2.410e−01	–	3.767e−02	–	3.036e−02	–	4.027e−03	–
8	1.181e−01	1.10	6.627e−03	2.68	3.296e−03	3.42	2.350e−04	4.38
12	7.697e−02	1.06	2.792e−03	2.14	9.435e−04	3.09	4.534e−05	4.07
16	5.788e−02	1.17	1.562e−03	2.38	3.948e−04	3.57	1.434e−05	4.72

Table 7
Errors and convergence rates for DS_r^{D} on $\mathcal{T}_h^2$.

n	$r=1$		$r=2$		$r=3$		$r=4$	
	Error	Rate	Error	Rate	Error	Rate	Error	Rate
L^2 errors and convergence rates								
4	7.509e−02	–	6.434e−03	–	3.634e−03	–	4.786e−04	–
8	1.797e−02	2.21	6.427e−04	3.55	2.242e−04	4.30	1.565e−05	5.28
12	7.626e−03	2.12	1.813e−04	3.13	4.441e−05	4.00	2.076e−06	4.99
16	4.349e−03	2.30	7.660e−05	3.53	1.433e−05	4.63	5.008e−07	5.83
H^1-seminorm errors and convergence rates								
4	2.410e−01	–	3.517e−02	–	2.527e−02	–	3.516e−03	–
8	1.181e−01	1.10	6.436e−03	2.62	3.127e−03	3.22	2.330e−04	4.19
12	7.697e−02	1.06	2.662e−03	2.18	9.180e−04	3.03	4.608e−05	4.01
16	5.788e−02	1.17	1.475e−03	2.42	3.913e−04	3.49	1.473e−05	4.67

where the supplemental space $\mathbb{S}_r^{DS}(E)$ was constructed for the sake of H^1-conformity. We developed the direct serendipity spaces for $r \geq 3$, where there are $3(r+1)$ linearly independent supplements, of which 12 are for separating edge DoFs, and the others are for the separation of face DoFs. We noted that not all of the supplemental functions on a cube are naturally generalized, since we required that the space restricted to each face coincides with a two dimensional direct serendipity space. The direct serendipity spaces on element E for $r = 1, 2$ were constructed as subspaces of $DS_3(E)$.

The spaces $DS_r(E)$ depend on our choice of nine special functions. Additional restrictions were required for the first six, λ_x, λ_y, λ_z, R_x, R_y, and R_z, in order to satisfy global H^1-conformity. For the other three, ψ_x, ψ_y, and ψ_z, their traces on ∂E were fully determined by λ_x, λ_y, λ_z, R_x, R_y, and R_z, and their definition in the interior could be decided in different ways, of which a few were presented in Section 7. The unisolvence of DoFs naturally follows from our development of basis functions.

The restriction of the finite elements to the faces gives a set of functions that are not merely polynomials. Rather, they are two-dimensional direct serendipity spaces. As such, two adjacent finite elements do not necessarily merge to form an H^1-conforming space. However, we noted that this can always be done in a straightforward manner if one uses a logically rectangular mesh.

The establishment of approximation properties closely followed [16,24,25] with a continuous dependence argument over a compact set of perturbations. An assumption on the regularity of the mesh was made. Moreover, the special functions used in the construction of the finite elements were required to be piecewise continuous and uniformly differentiable H^1 functions of the vertices of E. Under these assumptions, the optimal convergence rates were obtained for DS_r.

We conducted numerical tests for the finite element approximation of a Dirichlet problem on regularly and randomly distorted mesh sequences. For different choices of the special functions R_x, R_y, R_z, ψ_x, ψ_y, and ψ_z in Section 7 (smooth, marching tetrahedra, and diamond lattice cells), the performance of DS_r^S, DS_r^M, and DS_r^D were compared. They all converge at the expected rates on both mesh sequences, but DS_r^S with smooth supplements gives the best performance for higher r.

We close by noting that an open problem is to develop $H(\mathrm{div})$ and $H(\mathrm{curl})$ conforming mixed finite elements related by a de Rham complex to the direct serendipity finite elements constructed in this paper. We emphasize that they are not trivially found from the serendipity spaces. The finite element exterior calculus (FEEC) [18,31] suggests that the relevant de Rham sequence is

$$\mathbb{R} \hookrightarrow H^1 \xrightarrow{\mathrm{grad}} H(\mathrm{curl}) \xrightarrow{\mathrm{curl}} H(\mathrm{div}) \xrightarrow{\mathrm{div}} L^2 \longrightarrow 0, \tag{128}$$

wherein the new direct serendipity elements approximates the space H^1.

CRediT authorship contribution statement

Todd Arbogast: Writing – review & editing, Writing – original draft, Validation, Supervision, Software, Resources, Project administration, Methodology, Investigation, Funding acquisition, Formal analysis, Conceptualization. **Chuning Wang:** Writing – review & editing, Writing – original draft, Visualization, Validation, Software, Methodology, Investigation, Formal analysis, Conceptualization.

Funding

This work was supported by the U.S. National Science Foundation under grant DMS-2111159.

Declaration of competing interest

The authors declare that they have no known competing financial interests or personal relationships that could have appeared to influence the work reported in this paper.

Data availability

Data will be made available on request.

References

[1] E.L. Wachpress, A Rational Finite Element Basis, in: Mathematics in Science and Engineering, vol. 114, Academic Press, New York and London, 1975.
[2] C. Talischi, G.H. Paulino, A. Pereira, I.F. Menezes, Polygonal finite elements for topology optimization: a unifying paradigm, Int. J. Numer. Methods Eng. 82 (6) (2006) 671–698.
[3] A.L. Gain, G.H. Paulino, L.S. Duarte, I.F. Menezes, Topology optimization using polytopes, Comput. Methods Appl. Mech. Engrg. 293 (2015) 411–430.
[4] D.W. Spring, S.E. Leon, G.H. Paulino, Unstructured polygonal meshes with adaptive refinement for the numerical simulation of dynamic cohesive fracture, Int. J. Fract. 189 (2014) 33–57, http://dx.doi.org/10.1007/s10704-014-9961-5.
[5] J.E. Bishop, Applications of polyhedral finite elements in solid mechanics, in: Generalized Barycentric Coordinates in Computer Graphics and Computational Mechanics, CRC Press, 2017, pp. 179–196.
[6] D. Arnold, F. Brezzi, B. Cockburn, L. Marini, Unified analysis of discontinuous Galerkin methods for elliptic problems, SIAM J. Numer. Anal. 39 (2001) 1749–1779.
[7] A. Cangiani, E.H. Georgoulis, P. Houston, hp-version discontinuous Galerkin methods on polygonal and polyhedral meshes, Math. Models Methods Appl. Sci. 24 (10) (2014) 2009–2041.
[8] L. Mu, J. Wang, X. Ye, Weak Galerkin finite element methods on polytopal meshes, Int. J. Numer. Anal. Model. 12 (1) (2015) 31–53.
[9] A. Vaziri, J. Mora Paz, F. Fuentes, L. Demkowicz, High-order polygonal finite elements using ultraweak formulations, Comput. Methods Appl. Mech. Engrg. 332 (2018) 686–711.
[10] J.D.M. Paz, Polydpg: A Discontinuous Petroz-Galerkin Methodology for Polytopal Meshes with Applications to Elasticity (Ph.D. thesis), University of Texas at Austin, Austin, TX 78712, computational Science, Engineering and Mathematics (CSEM) Program, 2020.
[11] C. Bacuta, L. Demkowicz, J. Mora Paz, C. Xenophontos, Analysis of non-conforming DPG methods on polyhedral meshes using fractional Sobolev norms, Comput. Math. Appl. 95 (2021) 215–241, special Issue on Minimum Residual Methods.
[12] L. Demkowicz, J. Gopalakrishnan, A class of discontinuous Petrov–Galerkin methods. Part I: The transport equation, Comput. Methods Appl. Mech. Engrg. 199 (23–24) (2010) 1558–1572.
[13] F. Brezzi, K. Lipnikov, V. Simoncini, A family of mimetic finite difference methods on polygonal and polyhedral meshes, Math. Models Methods Appl. Sci. 15 (10) (2005) 1533–1551.
[14] L. Beirão da Veiga, F. Dassi, A. Russo, High-order virtual element method on polyhedral meshes, Comput. Math. Appl. 74 (5) (2017) 1110–1122.
[15] D.N. Arnold, G. Awanou, The serendipity family of finite elements, Found. Comput. Math. 11 (3) (2011) 337–344.
[16] T. Arbogast, Z. Tao, C. Wang, Direct serendipity and mixed finite elements on convex quadrilaterals, Numer. Math. 150 (2022) 929–974, http://dx.doi.org/10.1007/s00211-022-01274-3.
[17] T. Arbogast, C. Wang, Direct serendipity and mixed finite elements on convex polygons, Numer. Algorithms 92 (2023) 1451–1483, http://dx.doi.org/10.1007/s11075-022-01348-1.
[18] D.N. Arnold, R.S. Falk, R. Winther, Finite element exterior calculus, homological techniques, and applications, Acta Numer. 15 (2006) 1–155.
[19] S. Sun, J. Liu, A locally conservative finite element method based on piecewise constant enrichment of the continuous Galerkin method, SIAM J. Sci. Comput. 31 (4) (2009) 2528–2548.
[20] S. Lee, Y.-J. Lee, M.F. Wheeler, A locally conservative enriched Galerkin approximation and efficient solver for elliptic and parabolic problems, SIAM J. Sci. Comput. 38 (3) (2016) A1404–A1429.
[21] T. Arbogast, Z. Tao, A direct mixed–enriched Galerkin method on quadrilaterals for two-phase Darcy flow, Comput. Geosci. 23 (5) (2019) 1141–1160, http://dx.doi.org/10.1007/s10596-019-09871-2.
[22] P.G. Ciarlet, The Finite Element Method for Elliptic Problems, North-Holland, Amsterdam, 1978.
[23] A. Doi, A. Koide, An efficient method of triangulating equi-valued surfaces by using tetrahedral cells, IEICE Trans. Inf. Syst. 74 (1) (1991) 214–224.
[24] C. Wang, Direct Serendipity and Mixed Finiye Elements on Polygons and Cuboidal Hexahedra (Ph.D. thesis), University of Texas at Austin, 2023.
[25] T. Arbogast, C. Wang, Construction of supplemental functions for direct serendipity and mixed finite elements on polygons, Mathematics 11 (22) (2023) 4663, http://dx.doi.org/10.3390/math11224663.
[26] V. Girault, P.A. Raviart, Finite Element Methods for Navier-Stokes Equations: Theory and Algorithms, Springer-Verlag, Berlin, 1986.
[27] L.R. Scott, S. Zhang, Finite element interpolation of nonsmooth functions satisfying boundary conditions, Math. Comp. 54 (1990) 483–493.
[28] J.H. Bramble, S.R. Hilbert, Estimation of linear functionals on Sobolev spaces with applications to Fourier transforms and spline interpolation, SIAM J. Numer. Anal. 7 (1970) 112–124.
[29] T. Dupont, L.R. Scott, Polynomial approximation of functions in Sobolev space, Math. Comp. 34 (1980) 441–463.
[30] S.C. Brenner, L.R. Scott, The Mathematical Theory of Finite Element Methods, Springer-Verlag, New York, 1994.
[31] D.N. Arnold, R.S. Falk, R. Winther, Finite element exterior calculus: from hodge theory to numerical stability, Bull. Amer. Math. Soc. (N.S.) 47 (2) (2010) 281–354.